Soil Dynamics and Earthquake Engineering 42 (2012) 255–274

Contents lists available at SciVerse ScienceDirect

Soil Dynamics and Earthquake Engineering

journal homepage: www.elsevier.com/locate/soildyn

Constitutive model for soil amplification of ground shaking: Parameter calibration, comparisons, validation

Vasileios A. Drosos *, Nikos Gerolymos, George Gazetas

National Technical University, Athens, Greece

ARTICLE INFO

Article history:
Received 23 September 2011
Received in revised form
29 May 2012
Accepted 3 June 2012
Available online 15 July 2012

ABSTRACT

A one-dimensional constitutive model, developed for the nonlinear ground response analysis of layered soil deposits, is calibrated and validated experimentally in this paper. The small number of parameters renders the model easily implementable, yet quite flexible in effectively reproducing almost any type of experimentally observed hysteretic soil behavior. In particular, the model generates realistic shear modulus and damping curves as functions of shear strain, as well as stress–strain hysteresis loops. The model is calibrated against three sets of widely-used published shear modulus and damping ($G:\gamma$ and $\xi:\gamma$) curves and a library of parameter values is assembled to facilitate its use. The model, along with a developed explicit finite-difference code, NL-DYAS, for analyzing the wave propagation in layered hysteretic soil deposits, is tested against established constitutive models and numerical tools such as Cyclic1D [12] and SHAKE [42], and validated against experimental data from two centrifuge tests. Emphasis is given on the proper assessment of the V_s profile in the centrifuge tests, on the role of soil nonlinearity, and on comparisons of two inelastic codes (NL-DYAS and Cyclic1D) with equivalent linear (SHAKE) analysis.

1. Introduction

The paper addresses the problem of dynamic nonlinear analysis of the response of horizontally-layered soil deposits to seismic excitation. The latter is assumed to be the result of exclusively vertically-polarized *S* waves, and hence the analysis is reduced to 1-D wave propagation. Whereas in current worldwide state of practice the so-called equivalent-linear approximation [40,27] and the associated code 'SHAKE' [42] still dominate [46,4,3,47], numerous truly-nonlinear inelastic algorithms have been developed and publicized. They utilize numerous constitutive relations, ranging from purely empirical [24,33,19,31,36] to elaborate relations based on plasticity theory [5,35,6,34,30]. As has been pointed out by Steward et al. [45], whereas numerous studies have explored the sensitivity of the ground response to the equivalent-linear soil parameters [G_{max}, $G:\gamma$, $\xi:\gamma$] [41,28,29], the published information for the role of inelastic soil parameters is scarce.

In an earlier publication, Gerolymos and Gazetas [15] presented a 1-D phenomenological stress–strain model, 'BWGG', an extension of the Bouc–Wen constitutive law, which is quite versatile, capable of reproducing even some of the most complex nonlinear characteristics of cyclic behavior, including cyclic mobility and liquefaction.

In this paper, the 'BWGG' is reformulated and calibrated against published experimental soil data. To this end, a comprehensive methodology for the calibration of the model parameters is developed, so that the constitutive stress–strain loops are consistent with almost any pair of shear modulus and damping curves of the literature, while at the same time the corresponding experimentally observed hysteretic soil behavior is realistically reproduced.

Thereafter, the finite-difference wave-propagation code NL-DYAS, into which the model was implemented, is validated through a number of case studies. Its results are compared against those of the equivalent-linear code SHAKE [42] and the inelastic code Cyclic1D [12,13]. Finally, the three codes are utilized in a class C prediction (*i.e.,* knowing the results a-priori) of two centrifuge experiments [43]. Considerable insight is gained from these comparisons, and the need for reliable measurement of soil stiffness in the centrifuge (during-flight) is elucidated.

2. Brief model description

One-dimensional nonlinear constitutive models for soils are, mostly, of an empirical nature. They are not derived from fundamental physical laws, but they are meant to reproduce within engineering accuracy a relevant set of experimental stress–strain

* Corresponding author.
E-mail address: vadrosos@gmail.com (V.A. Drosos).

0267-7261/$ - see front matter © 2012 Elsevier Ltd. All rights reserved.
http://dx.doi.org/10.1016/j.soildyn.2012.06.003

relationships [20,37]. They are *phenomenological* models. For cyclic loading, involving unloading and reloading cycles, most available models are based on the Masing hypothesis ("criterion"). Many such models do not fit the experimental $G:\gamma$ and $\xi:\gamma$ curves simultaneously — often overestimating the hysteretic damping at large strains. In addition, in many cases they model rather crudely the shape of experimental stress–strain loops.

To avoid some of these drawbacks Gerolymos and Gazetas [15] adopted the model developed by Bouc [7] and Wen [51]. This model consists of a first order nonlinear differential expression that relates input (strain or displacement) to output (stress or force). The parameters that appear in the differential expression can be tuned to match either the hysteretic loops or a few simpler characteristics of relevant soil experiments. The model is quite versatile in reproducing a wide range of nonlinear material response to static and cyclic loading, including stiffness and strength degradation during cyclic loading [15–17]. Gerolymos and Gazetas [15] extended the original model to simulate a few fairly complex characteristics of cyclic soil behavior, and implemented the model into a nonlinear 1D wave-propagation algorithm, NL-DYAS.

It is stressed here, that one of the main advantages of the aforementioned wave-propagation algorithm against its numerous

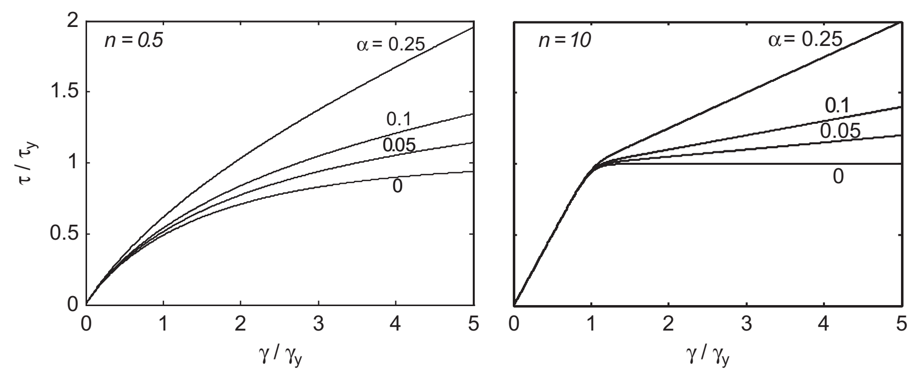

Fig. 1. Range of stress–strain monotonic "backbone" curves of the developed model: influence of parameters n and α.

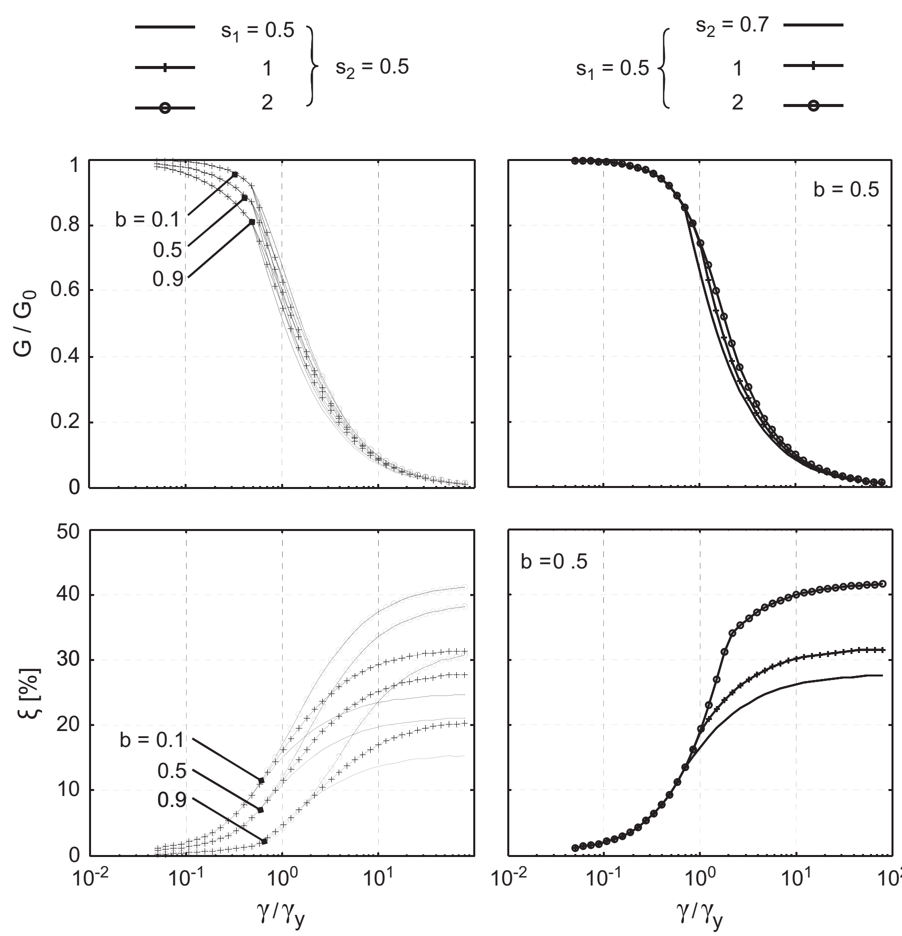

Fig. 2. Range of $G:\gamma$ and $\xi:\gamma$ curves for characteristic values of s_1 (left column) and s_2 (right column) [constant parameters $n=1$, $a=0$]. Notice the coincidence of G–γ curves for the different values of s_1 (top left chart).

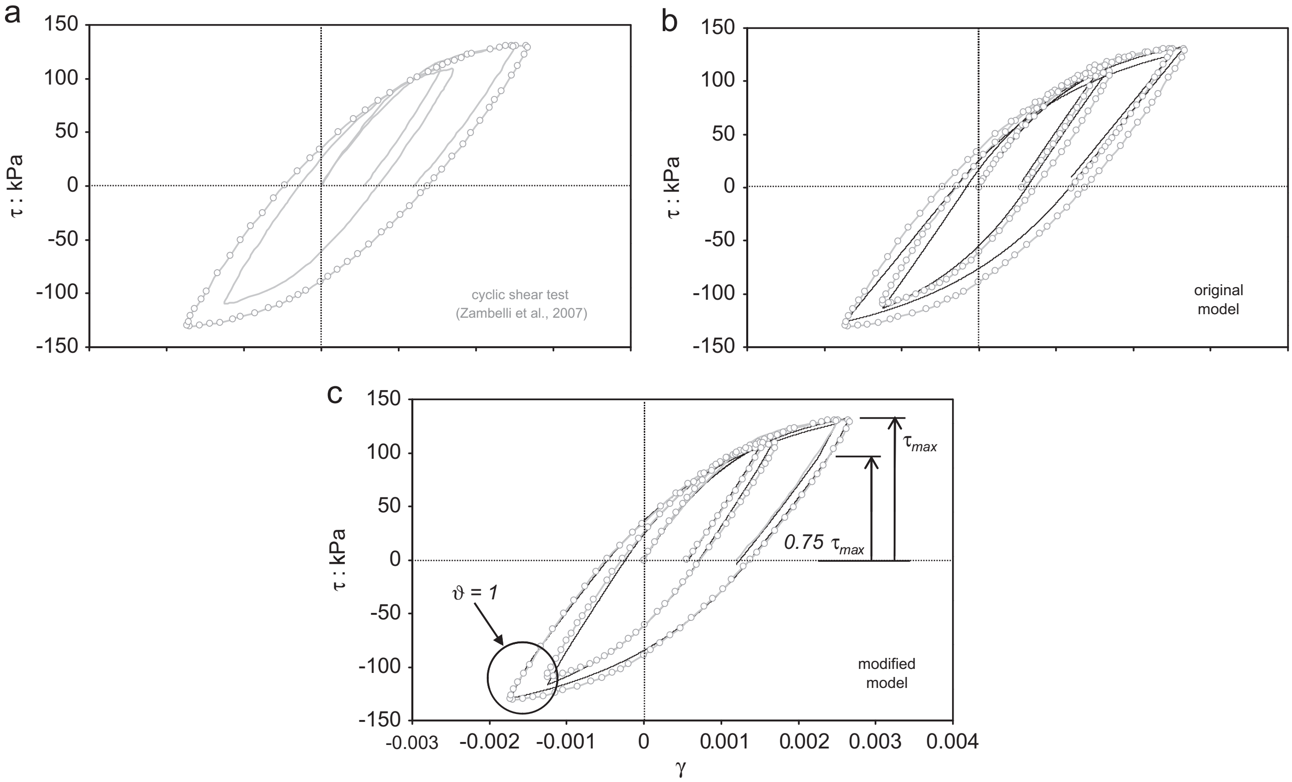

Fig. 3. Stress–strain loops of a dense Toyoura sand specimen: (a) experimentally measured [Zambelli et al., [54]] ; (b), (c) calculated with the BWGG constitutive model : (b) for zero yield shear stress at zero plastic strain, and (c) for a yield shear stress equal to 25 % of the maximum shear stress at the most recent stress reversal (the parameter values used for the production of the loops above are the same for both cases).

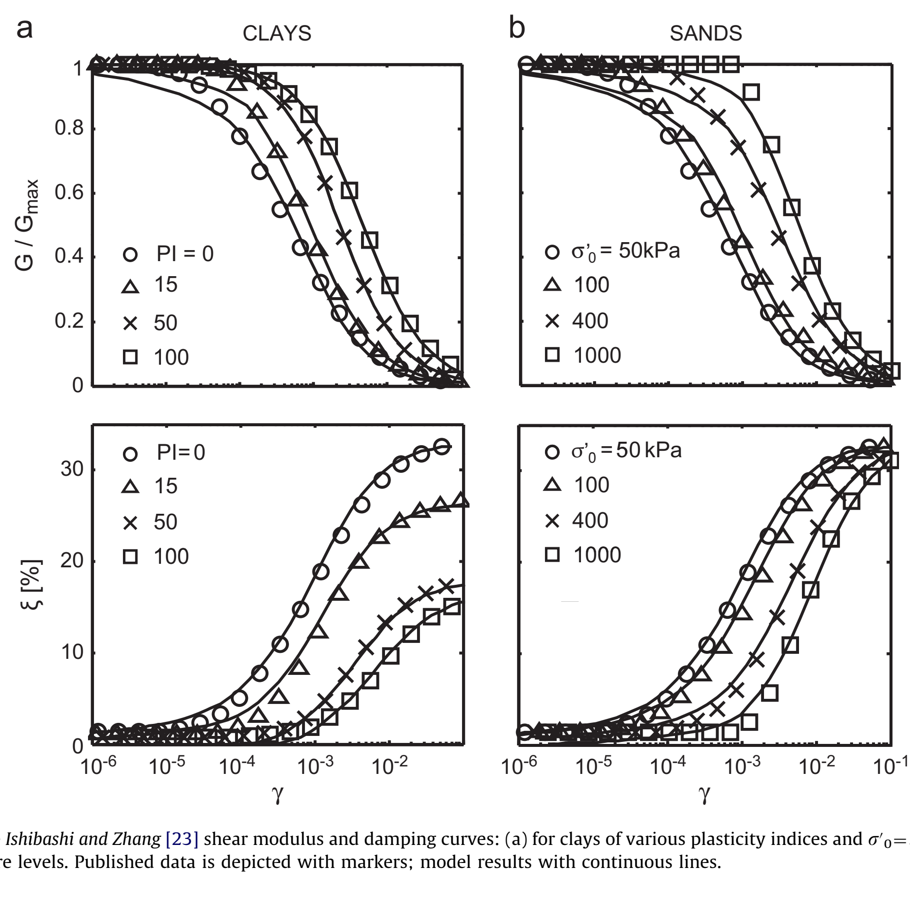

Fig. 4. Approximation of the *Ishibashi and Zhang* [23] shear modulus and damping curves: (a) for clays of various plasticity indices and $\sigma'_0 = 50$ kPa, (b) for sands ($PI = 0$) of various confinement pressure levels. Published data is depicted with markers; model results with continuous lines.

alternatives available in the literature hinges on its 'smooth' representation through a simple first order differential equation. Thus, it is suitable for nonlinear inverse problems (a major topic in geotechnical earthquake engineering) as it greatly reduces the usually high computational cost due to the associated sophisticated optimization procedures. For example, it would be ideal for being used in conjunction with an unscented Kalman filter [26], for which representation of the studied system through a set of first-order differential equations is a prerequisite.

The present paper, aims at introducing one new simple empirical improvement and then focus to: (i) on tuning the model parameters to match typical shear modulus and damping characteristics of clays and sands; (ii) on comparing the results of the calibrated NL-DYAS code (with the tuned soil model) against established nonlinear (Cyclic1D) and equivalent-linear (SHAKE) codes; and (iii) on testing the three models/codes against the results of centrifuge experiments.

It is pointed out that, as explained in a recent mathematically-oriented comprehensive monograph on the Bouc–Wen model by Ikhouane and Rodellar [21], there is no rigorous proof of convergence — just abundant justification based on numerical simulations. This, incidentally, is the case with most other nonlinear models, including the equivalent linear model (used in SHAKE).

Details of the model have been presented in Gerolymos and Gazetas [15], and only a brief outline is given here. For the 1-D wave propagation problem the imposed mode of deformation is simple shear. The relationship of shear stress $\tau(t)$ *versus* shear strain $\gamma(t)$ and shear-strain increment $\dot{\gamma}(t)=d\gamma/dt$ is given with the following two equations:

$$\tau(t)=\alpha G_{\max}\gamma(t)+(1-\alpha)\tau_y\zeta(t) \tag{1}$$

$$\frac{d\zeta}{dt}=\vartheta\left\{1-|\zeta|^n\left[b+g\ \mathrm{sign}\left(\frac{d\gamma}{dt}\zeta\right)\right]\right\}\frac{d\gamma}{dt} \tag{2}$$

The first term on the right-hand side of Eq. (1) is linear with an effective modulus ($\alpha G_{\max}$) equal to the plastic stiffness, while the second term is the hysteretic component. The "hysteretic parameter" ζ is a dimensionless restoring stress that governs the nonlinear response in the time domain. $G_{\max}$=the small-strain (elastic) shear modulus, τ_y and γ_y=the stress and strain at "initiation" of yielding ($\tau_y=G_{\max}\ \gamma_y$). Parameters n, b, and g are dimensionless parameters which control the shape of the stress–strain loop; *sign*( ) is the signum ($\pm$) function. Specifically, as illustrated in Fig. 1:

- Parameter α controls the post yielding shear stiffness of the monotonic response: $\alpha>0$ is for strain-hardening behavior.
- Parameter n controls the smoothness of the transition from the elastic to plastic regime during monotonic loading. For values of $n<1$ the transition from the one regime to the other is quite smooth, while for $n>5$ the τ–γ curve approaches the bilinear behavior.
- Parameters b and g define the unloading/reloading curve. For $b=1$ and $g=0$ the behavior is nonlinear but elastic: the stress–strain "loop" coincides with the (monotonic) backbone τ–γ curve — an unrealistic material behavior. As b tends to 0 the stiffness upon unloading tends to become twice the initial (at virgin loading) tangent stiffness — also unrealistic material behavior. In the special case of $b=g=0.5$ the initial and the upon-reversal stiffnesses coincide — the Masing criterion is recovered.
- The multiplier ϑ modifies the shape and size of the hysteretic loops and is given by:

$$\vartheta=\begin{cases}\frac{s_1+a(\mu_r-1)+s_2}{s_1+\mu_r}, & \mu_r>s_2\\ 1, & \mu_r<s_2\end{cases} \tag{3}$$

where: s_1 is a dimensionless parameter that controls the stiffness degradation upon stress reversal, s_2 is a characteristic value of "strain ductility" $\mu(=\gamma/\gamma_y)$ beyond which the effect of θ multiplier on stiffness degradation is activated, and μ_r is a reference strain ductility defined for every unloading or reloading cycle as the ratio of half the difference in strain γ between two previous reversals over the reference strain γ_y.

Gerolymos and Gazetas [15] elaborated some extensions of the Bouc–Wen model to account in a realistically-approximate way for: soil stiffness and strength degradation with number of cycles, response under conditions of cyclic mobility; and asymmetric response with respect to loading direction. These modifications are not further discussed herein. It is also clearly noticed that in this paper no pore-water pressure generation is considered. In the case of potentially liquefiable soil (saturated material under large strain), the full formulation of the model [15] should be used after appropriate calibration.

Table 1
Values of calibrated model parameters according to Ishibashi and Zhang [23] curves.

PI	σ'_0	γ_y^{-1}	*b*	*n*	s_1	s_2
0	10	3500	0.60	0.40	2.20	0.10
0	50	1400	0.60	0.40	2.20	0.10
0	100	900	0.60	0.40	2.10	0.20
0	200	500	0.60	0.40	2.10	0.20
0	400	300	0.60	0.45	2.10	0.20
0	1000	200	0.60	0.70	2.00	0.20
15	10	1400	0.60	0.50	1.30	0.10
15	50	800	0.60	0.50	1.30	0.10
15	100	600	0.60	0.60	1.30	0.10
15	200	500	0.60	0.60	1.30	0.10
15	400	400	0.60	0.65	1.30	0.10
15	1000	300	0.60	0.75	1.30	0.10
30	10	600	0.60	0.80	1.00	0.00
30	50	500	0.60	0.80	1.00	0.00
30	100	400	0.60	0.80	1.00	0.00
30	200	400	0.60	1.00	1.10	0.00
30	400	400	0.60	1.20	1.20	0.00
30	1000	400	0.60	1.20	1.20	0.00
50	10	400	0.60	1.20	0.90	0.00
50	50	350	0.60	1.20	0.90	0.00
50	100	350	0.60	1.20	0.90	0.00
50	200	320	0.60	1.20	0.90	0.00
50	400	320	0.60	1.20	0.90	0.00
50	1000	280	0.60	1.20	0.90	0.00
100	10	160	0.60	1.20	0.80	0.00
100	50	160	0.60	1.20	0.80	0.00
100	100	150	0.60	1.20	0.80	0.00
100	200	150	0.60	1.20	0.80	0.00
100	400	150	0.60	1.20	0.80	0.00
100	1000	150	0.60	1.20	0.80	0.00
200	10	70	0.60	1.20	0.80	0.00
200	50	70	0.60	1.20	0.80	0.00
200	100	70	0.60	1.20	0.80	0.00
200	200	70	0.60	1.20	0.80	0.00
200	400	70	0.60	1.20	0.80	0.00
200	1000	70	0.60	1.20	0.80	0.00

Table 2
Values of calibrated model parameters according to Vucetic and Dobry [50] curves.

PI	γ_y^{-1}	*b*	*n*	s_1	s_2
0	1900	0.60	0.50	1.20	0.00
15	750	0.60	0.45	0.85	0.00
30	180	0.60	0.30	0.40	0.03
50	70	0.60	0.30	0.30	0.03
100	35	0.60	0.30	0.25	0.03
200	20	0.60	0.30	0.25	0.03

One of the significant attributes of the (extended) model is its ability to reproduce the secant modulus reduction ($G:\gamma$) and the damping growth ($\xi:\gamma$) curves almost independently, as shown in Fig. 2. Decreasing values of s_1 and s_2 lead to lower values of damping ratio for large strain amplitudes. But, while the damping curves cover a broad range, the corresponding shear modulus curves fall within a very narrow band. Hence, by a suitable choice of γ_y the modulus reduction curve can match the experimental data; for realistic damping curve the parameters b, s_1 and s_2 must be properly calibrated.

However, the hysteretic loops obtained with the model in its original form deviates from experimentally obtained loops of cyclic laboratory tests ("reality"). Upon a stress reversal the obtained modulus is lower than in reality. Hence, the shape of stress–strain loop attains sharper edges than it should. To overcome this drawback, a very simple intuitive modification is proposed: the modulus upon reversal from a shear stress $|\tau_0|$ down/up to a shear stress $0.75|\tau_0|$ is taken equal to the initial tangent modulus G_{max}, as shown in Fig. 3. The resulting τ–γ loops are compared with the experimentally obtained stress–strain loops for Toyoura sand by Zambelli et al. [54]. The threshold of 75% was selected after sensitivity analyses, as a compromise between the need for realistic stiffness and damping curves at high strain on one hand and for reproduction of realistic stress–strain loops on the other. It is not a perfect solution; just a simple "engineering" correction.

3. Calibration of model parameters

To determine the parameters of the model (Eqs. (1)–(3)), G_{max} is first obtained (e.g., from resonant column tests, crosshole/downhole tests, *etc.*); then, the parameters n, b, s_1, and s_2 must be assessed.

The calibration is based on matching some established experimental $G:\gamma$ and $\xi:\gamma$ curves from the literature. To this end, the Lavenberg – Marquardt optimization procedure is used, available in mathematical code MATLAB. Three published families of $G:\gamma$, $\xi:\gamma$ curves have been utilized: (a) the Vucetic and Dobry [50] curves for clays as a function of their plasticity index *PI*, (b) the pressure (σ'_0)-dependent curves for sands of Ishibashi and Zhang

Table 3
Values of calibrated model parameters according to Darendeli [10] curves.

PI	σ'_0	γ_y^{-1}	*b*	*n*	s_1	s_2
0	25	2100	0.60	0.50	1.00	0.00
0	100	1400	0.60	0.55	1.00	0.00
0	400	900	0.60	0.60	0.90	0.00
0	1600	600	0.60	0.65	0.90	0.00
15	25	1600	0.60	0.50	1.00	0.00
15	100	1100	0.60	0.60	1.00	0.00
15	400	800	0.60	0.70	1.00	0.00
15	1600	550	0.60	0.80	1.00	0.00
30	25	1250	0.60	0.50	1.00	0.00
30	100	900	0.60	0.60	1.00	0.00
30	400	600	0.60	0.70	1.00	0.00
30	1600	400	0.60	0.80	1.00	0.00
50	25	900	0.60	0.45	1.00	0.02
50	100	650	0.60	0.55	1.00	0.02
50	400	400	0.60	0.60	0.90	0.02
50	1600	300	0.60	0.70	0.90	0.02
100	25	550	0.60	0.40	1.00	0.02
100	100	400	0.60	0.50	1.00	0.00
100	400	250	0.60	0.60	0.90	0.00
100	1600	150	0.60	0.60	0.90	0.00

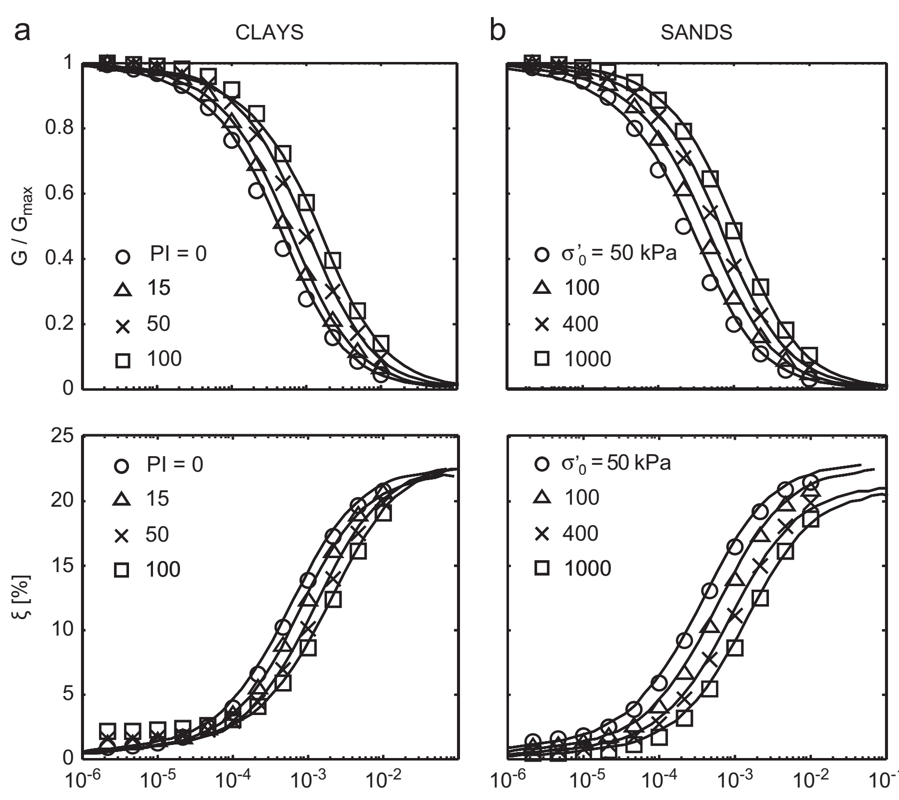

Fig. 5. Approximation of the Darendeli [10] shear modulus and damping curves: (a) for clays of various plasticity indices and σ'_0=100 kPa, (b) for sands (*PI*=0) of various confinement pressure levels. Published data is depicted with markers; model results with continuous lines.

[23], and (c) the Darendeli [10] curves, also functions of PI and σ'_0, the effective mean normal stress.

Based on the related sensitivity analysis, the useful range of each parameter is bounded as follows:

- Parameter n should take values between 0 and 5; with greater values the response approaches the bilinear elastoplastic, which is unrealistic.
- Parameter b should take values between 0.4 and 0.6, so that stress–strain loops resemble the observed experimental loops. Values close to 0 or 1 would lead to loops with very sharp edges — contrary to experimental observations.
- The post-yielding stiffness ratio α should be bounded between 0 and 0.02. It has been observed that greater values affect significantly the $G:\gamma$ and $\xi:\gamma$ curves. Hereafter, this strain-hardening parameter α is considered equal to 0.01, unless differently stated.
- s_1 should take values between 0 and 4; values greater than 4 result in large-strain damping ratio greater than 40% which is contrary to experiments for most soils.
- s_2 parameter can take any value greater than 0.
- The reference strain γ_y can take also any value between 10^{-5} and 10^{-1}.

Starting from the Ishibashi and Zhang [23] curves, six plasticity indices (PI=0, 15, 30, 50, 100, 200) and six mean confinement pressure levels (σ'_0=10, 50, 100, 200, 400, 1000 kPa) are examined. The results of the calibration are illustrated in Fig. 4 and the identified model parameters are given in Table 1. The agreement between computed and experimental curves is quite satisfactory. Small discrepancies are observed in the $G:\gamma$ curves for small strain levels, for plasticity indices varying from 0 to 30, and for both $G:\gamma$ and $\xi:\gamma$ curves for small strains and high confining

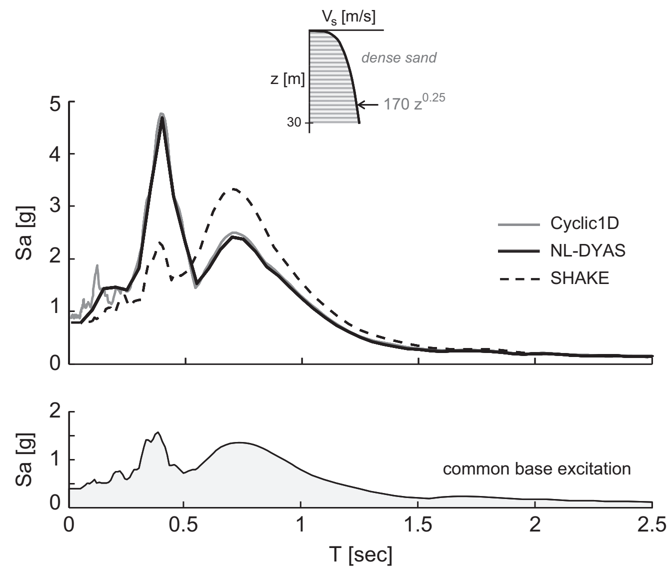

Fig. 7. Comparison of acceleration response spectra computed with the three models. Dense sand; shaking with Kobe JMA 090 record down-scaled to a_{base}=0.4 g.

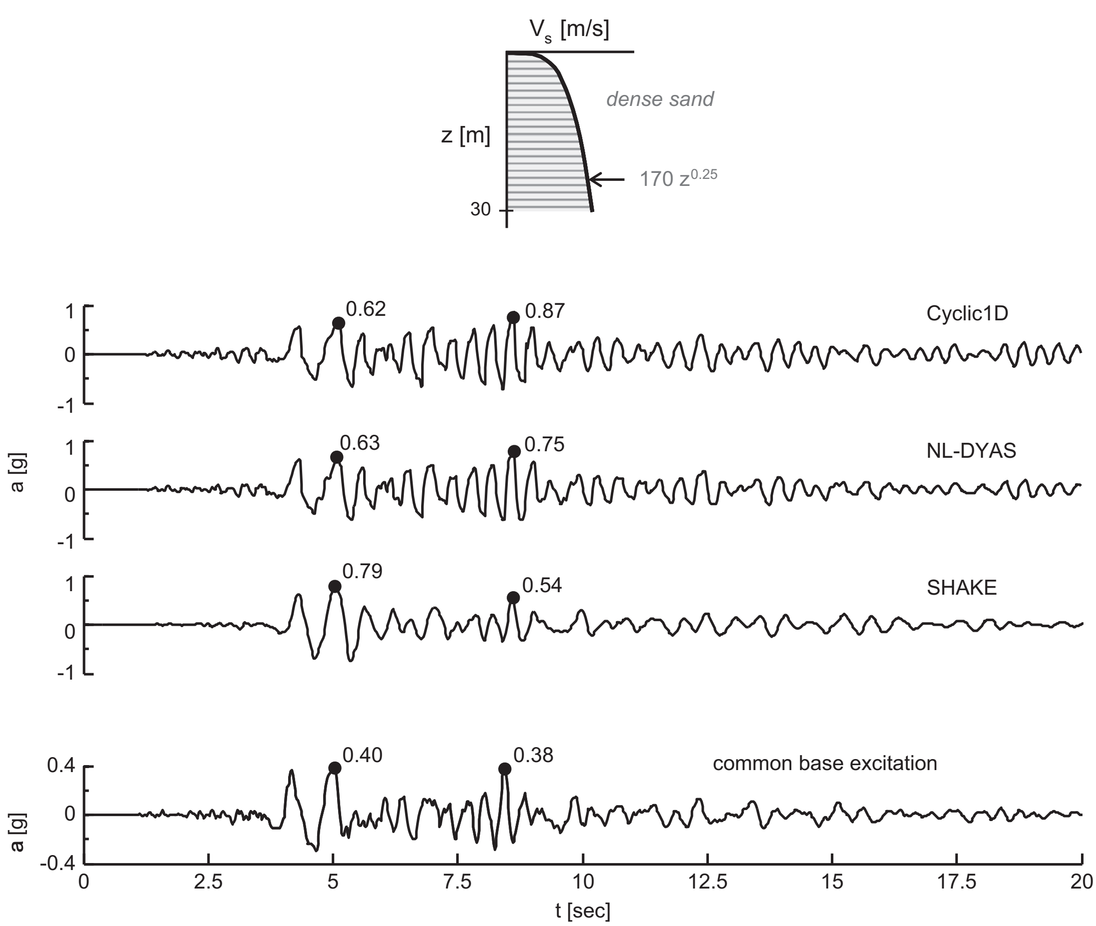

Fig. 6. Comparison of acceleration time histories computed with the three models. Dense sand; shaking with Kobe JMA 090 record down-scaled to a_{base}=0.4 g.

pressures. Table 1 summarizes the near-optimum values of the five parameters.

The same calibration procedure is utilized for the curves compiled by Vucetic and Dobry [50] which are only *PI*-dependent. Six pairs of curves are examined ($PI=0$, 15, 30, 50, 100, 200). Due to lack of space the results are not presented graphically, however the comparison of predicted to published curves is again reasonable. Table 2 summarizes the near-optimum values of the five parameters for reproduction of the aforementioned curves.

Darendeli [10] and Darendeli et al. [11] recommended a new family of normalized shear modulus and material damping curves, as functions of plasticity index and mean effective stress. Five plasticity indices ($PI=0$, 15, 30, 50, 100) and four confining pressures ($\sigma'_0=25$, 100, 400, 1600 kPa) are examined herein. Typical results of the calibration are illustrated in Fig. 5. The corresponding values for each parameter are summarized in Table 3. It is worth noticing in the 3 tables that the reference strain γ_y is a increasing function of the confining pressure and a generally increasing function of the plasticity index (with few exceptions).

It is noted that the calibration of the model parameters is not restricted to the suggested $G:\gamma$ and $\xi:\gamma$ curves matching procedure. Alternatively, it could be based on the direct

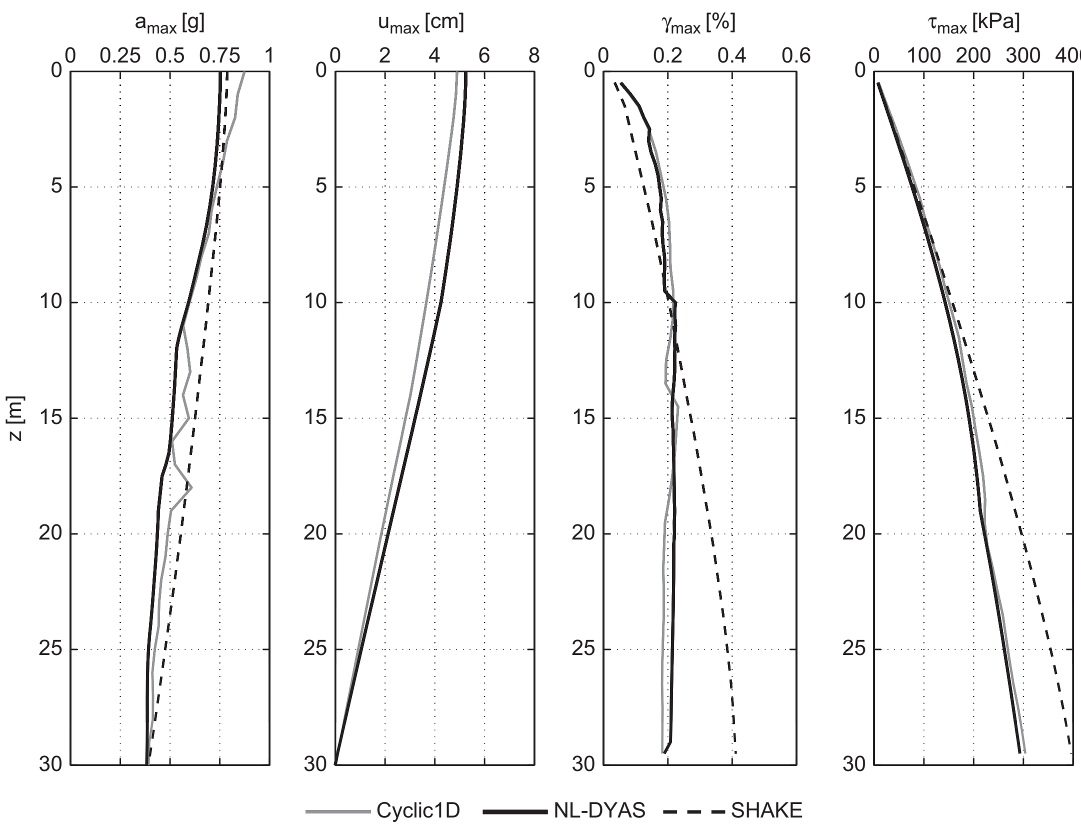

Fig. 8. Distributions of peak values of acceleration, shear strain, and shear stress computed with the three models. Dense sand; shaking with Kobe JMA 090 record down-scaled to $a_{base}=0.4$ g.

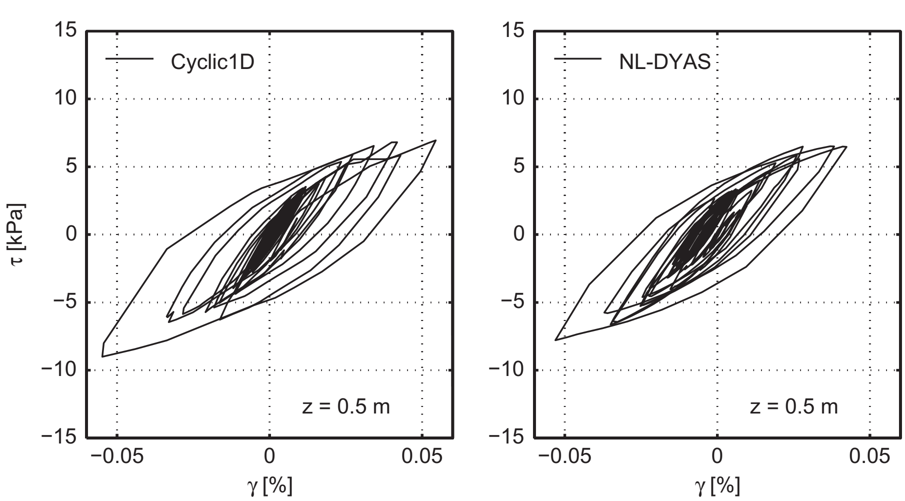

Fig. 9. Comparison of stress–strain loops computed with Cyclic1D and NL-DYAS. Dense sand; shaking with Kobe JMA 090 record down-scaled to $a_{base}=0.4$ g.

reproduction of experimental stress–strain loops with due consideration to asymmetric and hardening (or softening) response. Evidently, the applicability of the model is directly associated to the applicability of the data available for calibration.

For the seismic response of a layered soil deposit the model is incorporated into a finite-difference numerical scheme (code *NL-DYAS)* simulating the wave propagation through soil (*i.e.*, the differential equation of wave propagation is integrated numerically). This code is used herein for the 1-D seismic response analyses of soil deposits.

4. Comparisons against other numerical models

The effectiveness of the proposed model is checked against a sophisticated elastoplastic model. Elgamal et al. [12,13] and Yang et al. [52] based on the original multi-surface plasticity framework of Prevost [38] proposed an improved model for dynamic soil response analysis — capable of simulating even cyclic mobility and liquefaction. The model is implemented in a finite element code named *Cyclic1D* which can execute one-dimensional site amplification and liquefaction simulations, for level as well as mildly-inclined sites [12].

To compare NL-DYAS with Cyclic1D, the following two soil deposits are excited at their base and their response is calculated:

(a) a 30-m deep *dense sand* profile with density $\rho=2.1$ Mg/m^3, constant with depth, and shear wave velocity varying with depth according to $V_s \approx 170\,z^{0.25}$.
(b) a 30-m deep *soft clay* profile with density $\rho=1.3$ Mg/m^3, shear wave velocity $V_s=100$ m/s, and undrained shear strength $S_u=20$ kPa, all constant with depth.

These material properties were selected from the Cyclic1D built-in library of predefined materials.

Scaled versions of the JMA 090 record from the Kobe (1995) earthquake are used as excitation at the base of the soil columns.

We consider the sand to behave according to the Ishibashi and Zhang curves for $PI=0$, and the clay to follow the Vucetic and

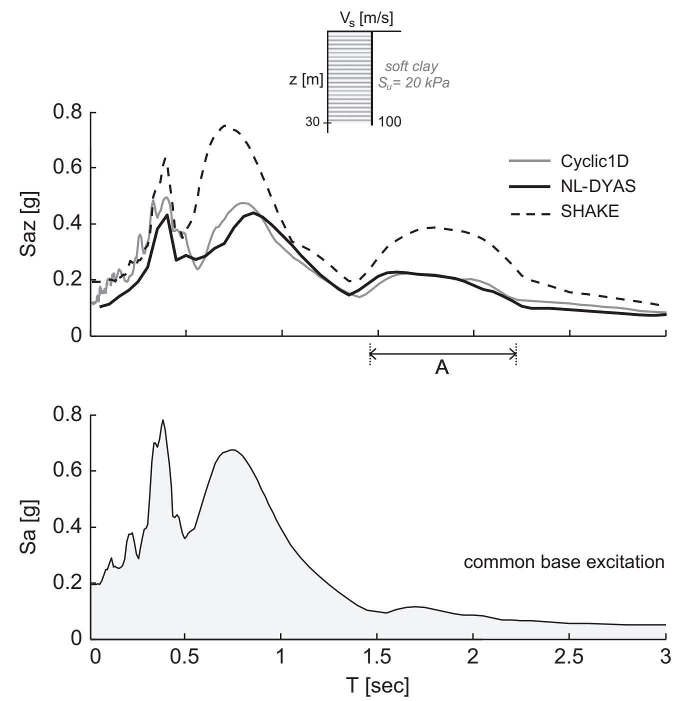

Fig. 11. Comparison of acceleration response spectra computed with the three numerical methods. Soft clay; shaking with Kobe JMA 090 record down-scaled to $a_{\text{base}}=0.2$ g.

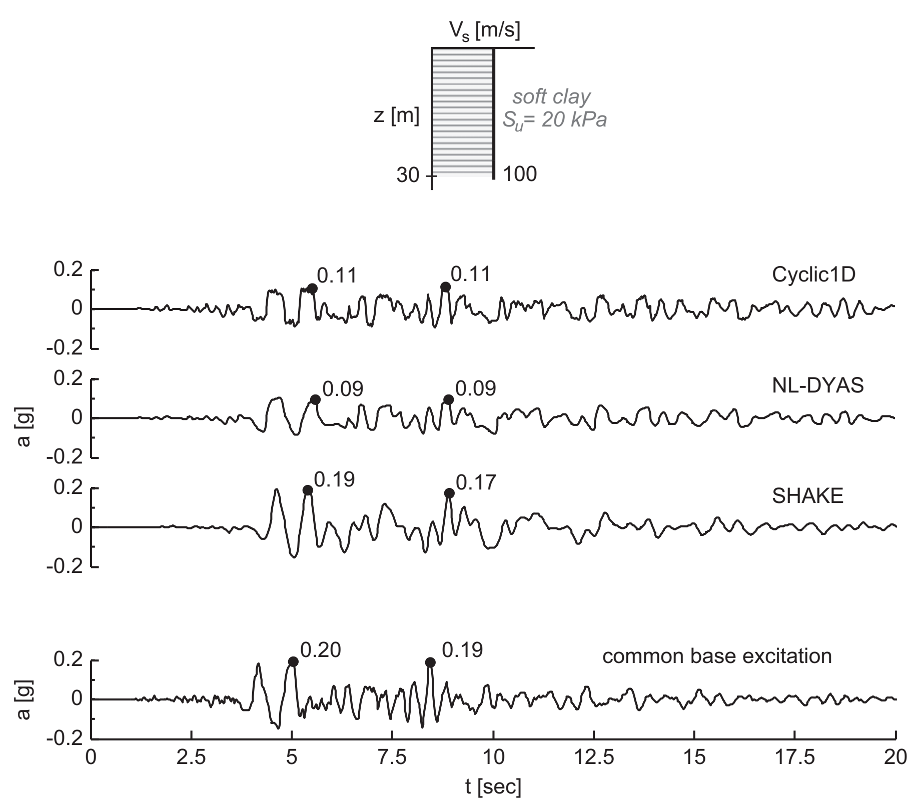

Fig. 10. Comparison of acceleration time histories computed with the three numerical methods. Soft clay; shaking with Kobe JMA 090 record down-scaled to $a_{\text{base}}=0.2$ g.

Dobry curves for $PI=30$. The corresponding soil parameter values are selected from Tables 1 and 2, respectively.

To serve as a yardstick, an equivalent linear soil response analysis was also carried out with the use of code SHAKE — the current state-of-practice soil amplification code.

4.1. First example: Dense sand deposit

The deposit is excited by the JMA record down-scaled to a peak acceleration of 0.4 g. The results of the three analyses (NL-DYAS, Cyclic1D, SHAKE) are portrayed in terms of: (a) the acceleration time histories at the ground surface (Fig. 6), (b) the corresponding acceleration response spectra (Fig. 7), (c) the distributions with depth of the peak values of acceleration, displacement, shear strain, and shear stress (Fig. 8), and (d) the stress–strain hysteresis loops of the two nonlinear models at a depth of 0.5 m (Fig. 9). The following conclusions can be drawn:

1. All three codes (and corresponding soil models) predict an amplification of the main long-period pulses of the excitation (occurring from about 4 to 5.5 s). The main difference is that whereas SHAKE gives an amplification by a factor of 2, NL-DYAS and Cyclic1D result in a nearly identical amplification by a factor of about 1.7.
2. The short-period oscillatory motion (occurring from about 7 to 9 s) is amplified by different factors, as follows:

- Cyclic1D: 2.23
- NL-DYAS: 1.92
- SHAKE: 1.35

3. The above two conclusions indicate a fairly similar response of Cyclic1D and NL-DYAS. On the other hand, SHAKE slightly exaggerates the long-period pulses, while it depresses the high-frequency components — a performance within expectations, as such "depression" of high frequencies has been already noted in the literature (*e.g.,* [8,3,49,39]). The response acceleration spectra from the three codes reinforce this conclusion: whereas the two inelastic soil models produce almost identical spectra (except in the period range around 0.1 s), the equivalent-linear analysis, having filtered-out the short-period components, underpredicts the spectral values for periods less than 0.55 s — in fact by a factor of 2 at $T\approx 0.4$ s.
4. The distributions with depth of the peak values of acceleration, shear stress, and horizontal displacement computed with the three codes are for all practical purposes identical (SHAKE does not produce output displacements). Peak shear strain is an exception: the two inelastic codes compute a fairly uniform distribution *versus* depth, at least for $z>5$ m, compared to an almost linear increase predicted with an equivalent linear analysis.

Table 4
Properties of Nevada sand used in centrifuge experiments at UC Davis (after [22]).

Parameter	*Value*
Soil type	Nevada sand
Specific gravity (Mg/m^3)	2.67
Mean grain size, D_{50} (mm)	0.17
Coefficient of uniformity, C_u	1.64
Maximum dry unit weight (kN/m^3)	16.9
Minimum dry unit weight (kN/m^3)	13.9
Maximum void ratio	0.887
Minimum void ratio	0.511

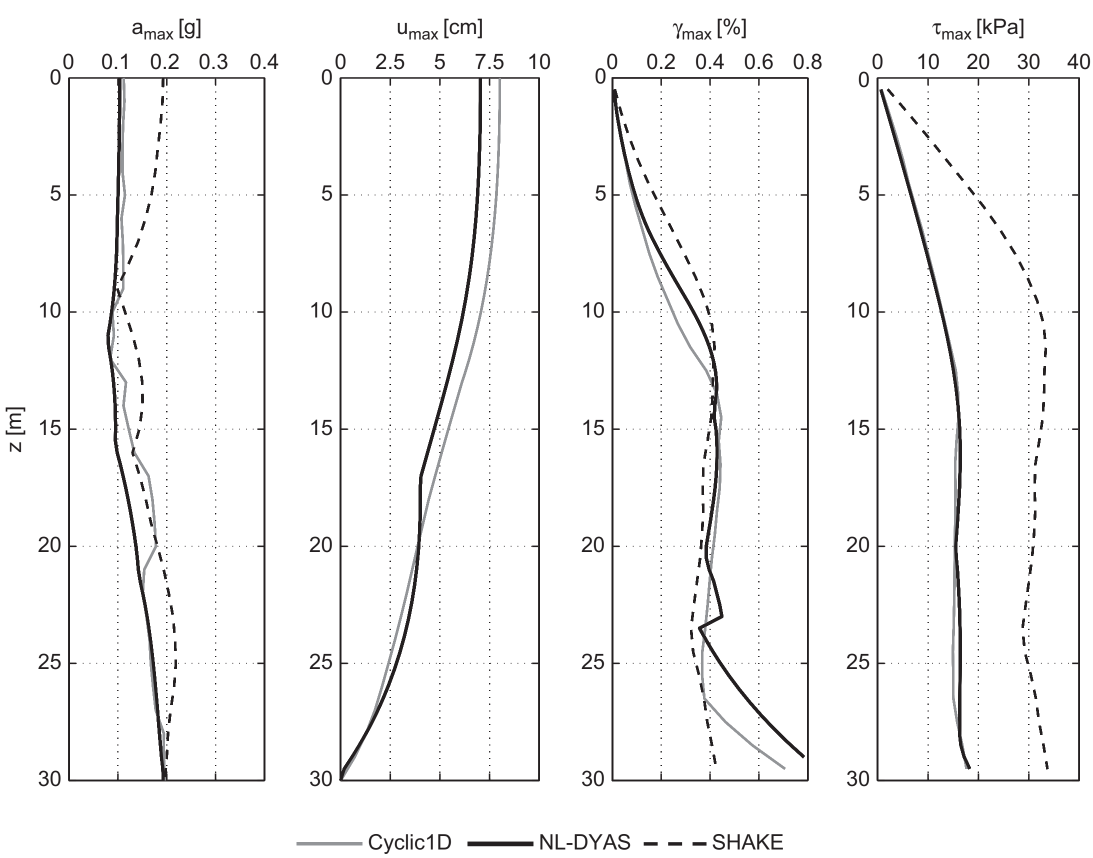

Fig. 12. Distributions of peak values of acceleration, shear strain, and shear stress computed with the three numerical methods. Soft clay; shaking with Kobe JMA 090 record down-scaled to $a_{base}=0.2$ g.

5. The similarity between the τ–γ diagrams of Cyclic1D and NL-DYAS analyses is evident. We note the slightly broader Cyclic1D hysteresis loop during the largest cycle. Contrasting with similar comparisons in the literature between τ–γ curves computed with various methods or determined experimentally, the agreement is judged quite satisfactory.
6. Given the sufficiently–inelastic response ($\gamma \approx 2 \times 10^{-3}$) of this strongly inhomogeneous soil profile (modulus *nearly* vanishing at the ground surface — fortunately not *exactly* thanks only to the unavoidable discretization in all analyses) the performance of the equivalent linear approximation is, in the authors' opinion, acceptable from a purely engineering point of view. It is worth mentioning that an improved equivalent-linear method that avoids the overdamping of high frequencies has been developed by Assimaki et al. [4] and Assimaki and Kausel [3]. Such overdamping stems from the facts that damping is a function of strain amplitude and that high frequencies are usually associated with small amplitudes of motion; thus, these components experience substantially less damping than the dominant frequencies and are artificially suppressed when hysteretic damping is taken as constant. And, of course, the discrepancies of the two inelastic methods are hardly noticeable to warrant a further discussion.

4.2. Second example: Soft and deep clay deposit

The soft clay deposit is excited at the base also by the JMA record but now down-scaled to a peak acceleration of 0.20 g. The results of the analyses are portrayed in Figs. 10–12 in the form of acceleration histories, response spectra, and distributions of peak values of response quantities with depth. The following remarks are worth making:

1. The two inelastic models show a clear deamplification of both the early long-period and the delayed short-period acceleration pulses (peak amplitudes reaching only about one-half of the corresponding peaks of the base acceleration). The equivalent-linear model predicts almost the same peak acceleration values as the base motion. These results are not surprising: 30 m of an S_u=20 kPa and $V_{S,0}$=100 m/s clay constitutes a very flexible homogeneous layer (initial elastic period $T_1 \approx 1.2$ s, increasing to nearly 2 s during shaking). Even an equivalent linear analysis should not lead to amplification, in view of the dominant periods of about 0.8 s (early pulses) and about 0.4 s (later pulses) of the excitation. On top of that, an S_u of merely 20 kPa would severely limit the transmitted acceleration — as it is observed in the square-like form of the long-period pulses at

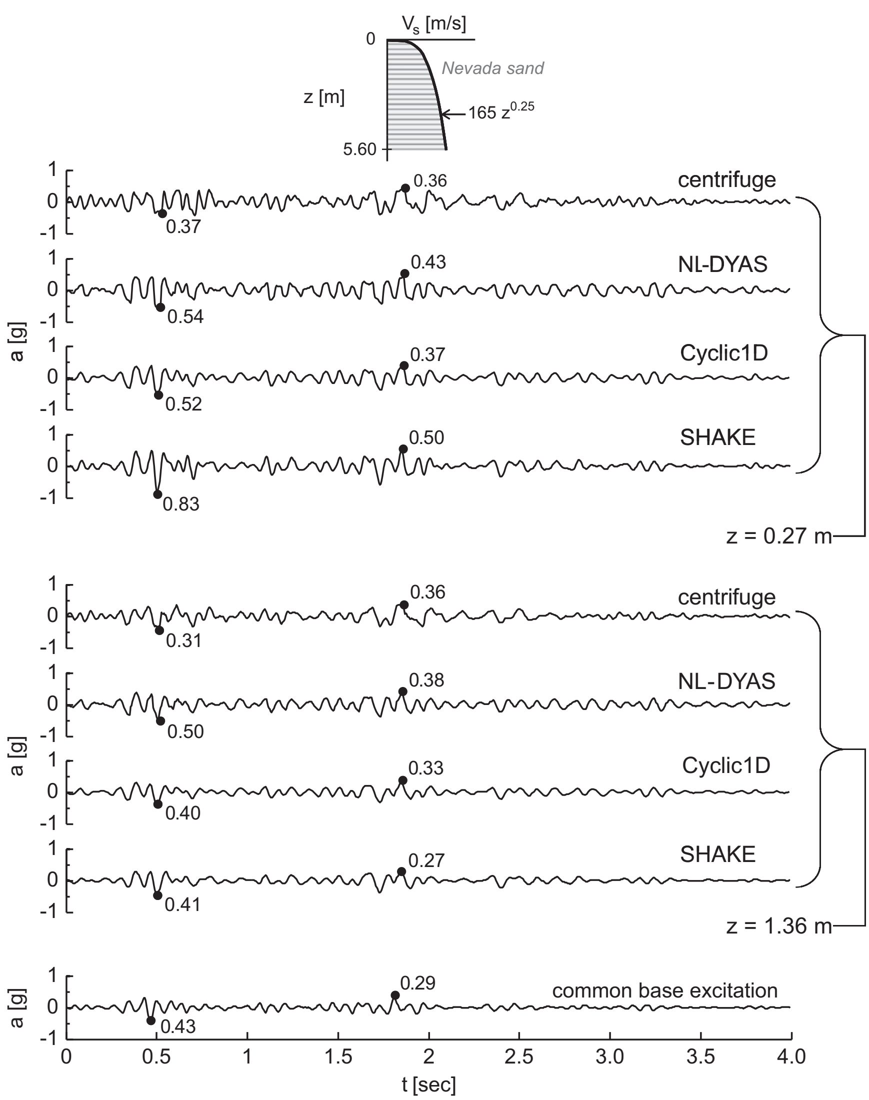

Fig. 13. Comparison of calculated and recorded acceleration time histories for DKS02 experiment (Originally suggested velocity profile: V_s=165 $z^{0.25}$; centrifuge acceleration 10 g; shaking with Santa Cruz record, Loma Prieta 1989).

the ground surface predicted by the two inelastic models. An equivalent-linear analysis cannot reproduce adequately this effect of soil plasticity.

2. Some of the above differences are reflected in the response acceleration spectra. Compared to the input spectrum, the inelastic models (Cyclic1D, NL-DYAS) produce an amplification by nearly a factor of 2 of the spectral values in the period range A (roughly between 1.45 and 2.20 s). At shorter periods the inelastic models lead to substantially smaller spectral values — by a factor of almost 2 for the peaks at $T \approx 0.35$ s and $T \approx 0.72$ s. The equivalent-linear SHAKE analysis gives a (surface) response spectrum which is very close to the input (base) spectrum at all periods, except at the period range A (1.45–2.20 s) where it produces about 3.5 times larger spectral values, approximately.
3. The spectrum of the equivalent-linear analysis exceeds the two inelastic-analyses spectra throughout the examined period range. The differences are negligible (or even non-existing) at very short periods around $T \approx 0.30$ s, and highest at $T \approx 0.72$ and $T \approx 1.8$ s.
4. Whereas the two inelastic analyses give practically the same distributions of peak stresses, accelerations, strains, and relative displacements, equivalent-linear analysis overpredicts them by a factor of nearly 2 in the crucial upper 5 or 10 m from the surface.
5. The two inelastic models, encoded in Cyclic1D and NL-DYAS, give practically identical results for this particular soil profile.

5. Validation against centrifuge model tests

During the last decades centrifuge soil testing has been proven to be an insightful method for understanding mechanisms governing dynamic soil performance and a valuable tool for calibrating theoretical models. Of course, in the limited soil domain tested in the centrifuge it is likely that 2-D wave propagation effects might develop and perturb the 1-D wave free field. To diminish such effects laminar soil containers are utilized, the vertical walls of which deform in horizontal shear, mimicking the shear wave deformation of the free field soil. Centrifuge testing remains the most accurate experimental method for soil systems, especially suited for research. One of its limitations, however, is the difficulty in determining (in-flight, of course) the precise stiffness and strength of soil *versus* depth.

Stevens et al. [43] reported on a series of tests in the 9-m radius centrifuge of the University of California at Davis investigating the nonlinear response of soil deposits to earthquake ground shaking.

Their DKS02 experiment offered a comprehensive investigation of nonlinear site response. A soil deposit consisting of a 0.6-m thick layer of dry Nevada sand (properties summarized at Table 4) with a relative density of about 100% and a unit weight of 16.8 kN/m^3 was installed in a laminar container and tested in the centrifuge with parametrically varying (radial) acceleration, 10, 20, and 40 g, thus simulating three deposits of thickness: 5.6 m, 11.2 m, and 22.4 m, respectively. Measuring the time delay in the arrival of traveling shear waves caused by an air-hammer shock at the base of the deposit, the small-strain shear wave velocity V_s was estimated by Stevens et al. [44] to vary with depth z according to:

$$V_s \approx 165\, z^{0.25} \ [\mathrm{m/s; m}] \tag{4}$$

Shaking was applied parallel to the long sides of the model container. A total of 98 shaking events were applied to the model, including various frequency sweeps and scaled versions of the Santa Cruz ground motion recorded in the 1989 Loma Prieta earthquake. Their results for the case of Santa Cruz excitation (peak acceleration at base 0.40 g) are utilized herein to check the reliability of the developed constitutive model. Instrumentation included longitudinal, transverse, and vertical accelerometer arrays, as well as horizontal and vertical displacement transducers.

This experiment (DKS02) was selected because: (a) it is well documented with data publicly available, and (b) it involves deposits of the same material but of different thickness — hence, giving the opportunity to test the models against different cases.

The ground response recorded in the central vertical array during the tests with centrifugal accelerations of 10 g and 20 g, seismically excited at the base by the Santa Cruz record, is compared to the NL-DYAS results, as well as the results of Cyclic1D (inelastic model) and SHAKE (equivalent-linear model).

To simulate the Nevada sand layer using NL-DYAS, the soil deposit is discretized into 17 layers. The V_s profile is given by Eq. (4) and the dynamic properties of sand are simulated according to Ishibashi and Zhang [23] curves for $PI=0$. Hence, the model parameters of Table 1 are used in the analysis. The centrifuge recorded base motion serves as (the common) base excitation, of all types of analyses.

5.1. Comparisons for the shallowest deposit ($H=5.6$ m)

The results are displayed in Fig. 13 (acceleration time histories) and Fig. 14 (corresponding response spectra). Evidently, the performance of the models is not particularly satisfactory. The peaks of the inelastic (NL-DYAS and Cyclic1D) accelerograms exceed those of the recorded motions near the ground surface: 0.54 g and 0.52 g, respectively (*versus* 0.37 g), for the first sequence of strong pulses. For the second sequence of strong pulses the discrepancies are smaller: 0.43 g and 0.37 g (*versus* 0.36 g). Discrepancies in the frequency content between the theoretical time histories and the records are also noticeable, especially in the time window between $t \approx 1.7$ s and $t \approx 2.6$ s,

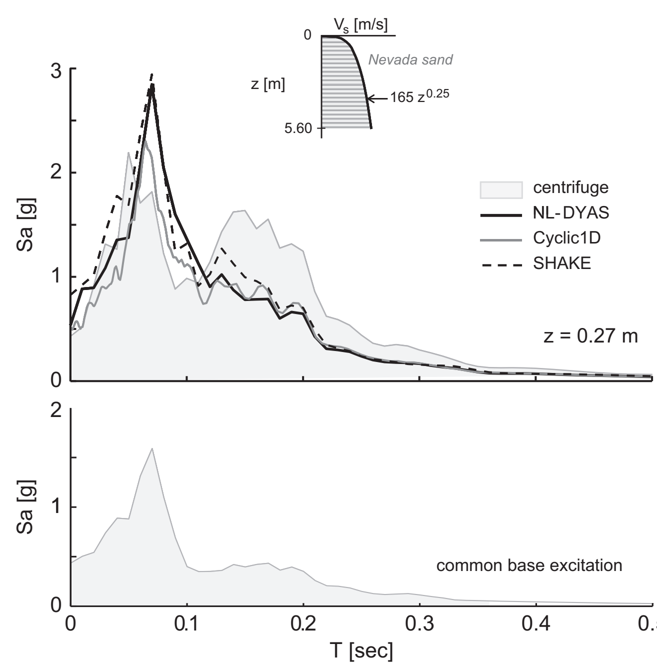

Fig. 14. Comparison of calculated and recorded acceleration response spectra for DKS02 experiment (Originally suggested velocity profile: $V_s=165\ z^{0.25}$; centrifuge acceleration 10 g; shaking with Santa Cruz record, Loma Prieta 1989).

where the centrifuge motions exhibit longer-period oscillations. Similar discrepancies in frequency content are conspicuous in the motions at the depth of $z=1.36$ m: the record displays substantially longer oscillation periods than the analyses.

Interestingly, the equivalent-linear (SHAKE) analysis leads to a near-surface accelerograms that exhibit nearly the same frequency content with the inelastic motions — thereby also in disparity with the content of the centrifuge record. The highest values of the peaks (0.83 and 0.50 g) are higher than those of all NL-DYAS, Cyclic1D and the record. But notice that especially the 0.83 g is nearly a solitary peak, with small perhaps influence on the response spectral values, beyond of course, the $T\approx 0$ region.

Overall, the agreement between analyses and experiment cannot be judged as satisfactory, at least for such a (seemingly) well controlled experiment.

The near-surface acceleration response spectra portray in a more conspicuous way the difference noticed in time histories. One can readily see that the spectrum of the centrifuge record exceeds by a factor of almost 1.8 the three theoretical spectra in the period range of 0.12 s to 0.27 s. We can "read" from the centrifuge time history that in the time interval $t\approx 1.8$–2.0 s the dominant (period) is about 0.16 s — i.e., in the middle of the above period range. At about the same time interval we can read from all the theoretical time histories a dominant period of about 0.075 s — no surprise therefore that the three (different in many respects) theoretical methods give the same sharp peak in S_a only at about $T\approx 0.08$ s, whereas the recorded spectrum has a (much flatter) significant peak at about 0.13 to 0.20 s, in addition to its peak at about 0.3 s.

One wonders: could the centrifuge results be interpreted differently? The quality of these results is beyond doubt. But the measurement of the dynamic shear modulus at various depths, on which all analyses hinge, are unavoidably imperfect (indirect *in-situ* measurements during spinning). Is it perhaps possible that the soil deposit was less stiff than what has been *estimated* by Stevens et al. [44]?

Using the Nevada sand properties and the Arulnathan et al. [2] measured V_s profile for $D_r=80\%$, *obtained in the same laboratory at UC Davis*, we suspect that the Stevens et al. [44] measurements of V_s may overestimate reality. Indeed, based on the soil

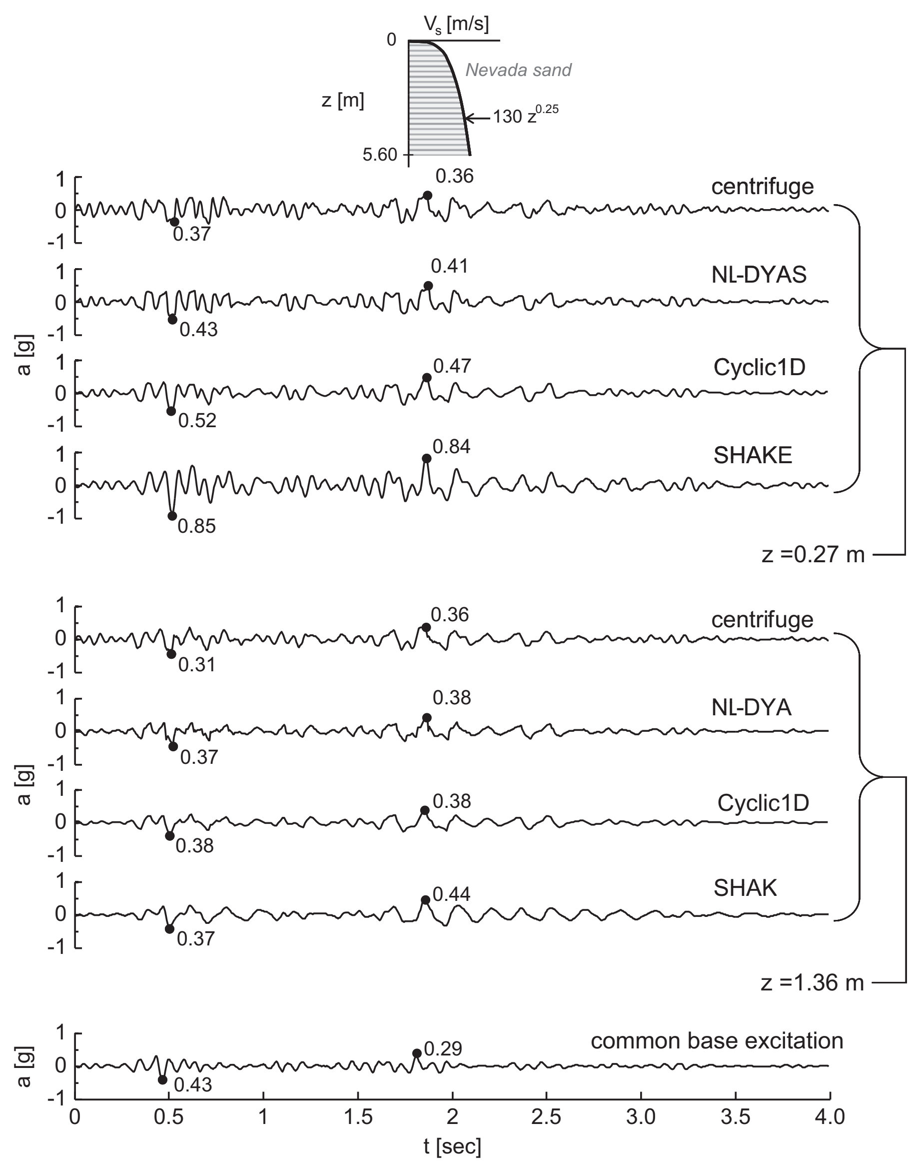

Fig. 15. Comparison of calculated and recorded acceleration time histories for DKS02 experiment (Revised velocity profile: $V_s=130\ z^{0.25}$; centrifuge acceleration 10 g; shaking with Santa Cruz record, Loma Prieta 1989).

properties of Table 4, the void ratio e of a Nevada sand deposit with D_r=80% is

$$e = e_{\max} - D_r(e_{\max} - e_{\min}) = 0.887 - 0.8(0.887 - 0.511) = 0.586 \quad (5)$$

According to Hardin [18], the maximum shear modulus for clean sand is expressed as

$$G_{\max} = \frac{625}{0.3+0.7e^2} p_a^{0.5} \sigma_m'^{\,0.5} \quad (6)$$

where p_a is the atmospheric pressure and σ_m' the mean effective stress. Hence, a Nevada sand deposit of D_r=100% (and hence $e \approx e_{\min}$=0.511), compared to a D_r=80% deposit, would have a zero-strain shear modulus

$$\frac{G_{\max}^{(100)}}{G_{\max}^{(80)}} = \frac{0.3+0.7e_{80}^2}{0.3+0.7e_{100}^2} = 1.15 \quad (7)$$

and a corresponding shear wave velocity

$$\frac{V_s^{(100)}}{V_s^{(80)}} = \sqrt{\frac{G_{\max}^{(100)}}{G_{\max}^{(80)}}} = \sqrt{1.15} = 1.07 \quad (8)$$

Arulnathan et al. [2] measured the V_s profile of a D_r 80% Nevada sand layer and fitted the expression

$$V_s \approx 120\, z^{0.25}\ [\mathrm{m/s; m}] \quad (9)$$

Therefore, a 100% dense Nevada sand layer is more likely to have a V_s given by

$$V_s \approx 1.07\ x\ 120 \approx 130\, z^{0.25} [\mathrm{m/s; m}] \quad (10)$$

We would have arrived to the same result if we had used the Jamiolkowski et al. [25] empirical expression for shear modulus

$$G_{\max} = \frac{625}{e^{1.3}} p_a^{0.5} \sigma_m'^{\,0.5} \quad (11)$$

and therefore

$$\frac{G_{\max}^{(100)}}{G_{\max}^{(80)}} = \frac{e_{80}^{1.3}}{e_{100}^{1.3}} \approx 1.20 \quad (12)$$

from which

$$\frac{V_s^{(100)}}{V_s^{(80)}} = \sqrt{\frac{G_{\max}^{(100)}}{G_{\max}^{(80)}}} \approx \sqrt{1.20} \approx 1.09 \quad (13)$$

and finally

$$V_s \approx 1.09\ x\ 120 \approx 130\, z^{0.25} [\mathrm{m/s; m}] \quad (14)$$

This (practically) coincidence of the above two V_s profiles strongly supports the claim that Eq. (4) exaggerates V_s, and that Eq. (14) is a more realistic choice. After re-estimating the soil stiffness based exclusively on additional experimental data *from the same UC Davis laboratory* and well-established empirical relations from the literature, we hence utilized this variation with depth instead of Eq. (4). Figs. 15–17 depict the results of the new analyses for centrifuge acceleration of 10 g (hence, H=5.6 m). Now the inelastic acceleration time histories compare

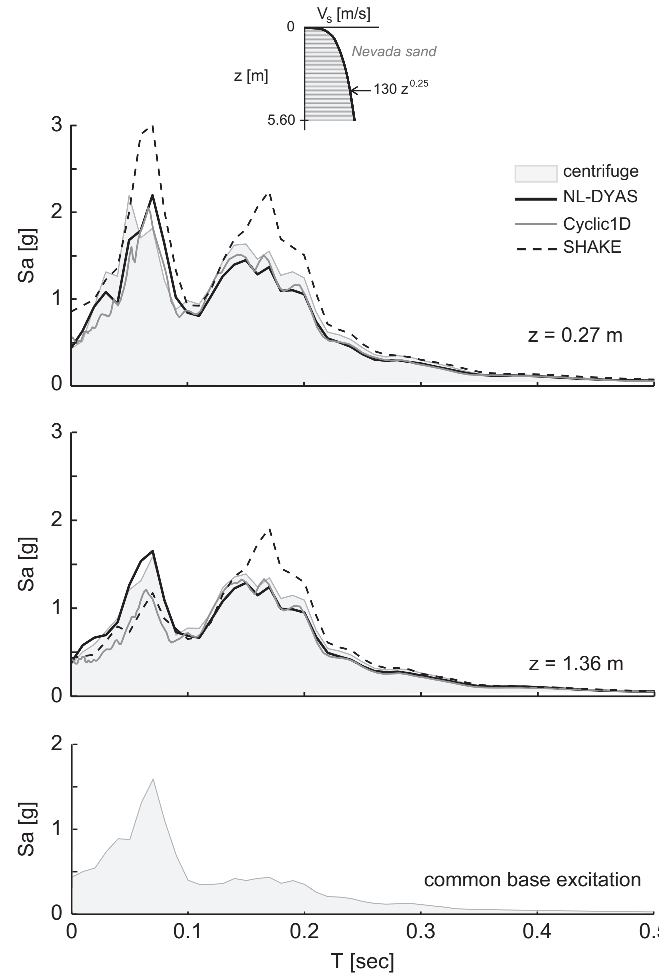

Fig. 16. Comparison of calculated and recorded acceleration response spectra for DKS02 experiment (Revised velocity profile: V_s=130 $z^{0.25}$; centrifuge acceleration 10 g; shaking with Santa Cruz record, Loma Prieta 1989).

better with the recorded motions both in amplitude and frequency content, at both depths (0.27 and 1.36 m). The equivalent linear motion still exhibits higher peaks (Fig. 15). In terms of response spectra (Fig. 16) the two inelastic codes (NL-DYAS and Cyclic1D) produce spectral values almost identical to the measured ones for the whole period range.

The equivalent linear method predicts similar frequency content with the recorded motion, although it overestimates the peak acceleration values: ground motion $PGA \approx 0.85$ g instead of 0.40 g, and spectral $S_{a,\max} \approx 3$ g instead of 2.1 g). In Fig. 17, the peak acceleration, shear strain, and shear stress profiles are presented. Notice the good accord of the two inelastic codes with the experimental peak accelerations at six depths. No experimental measurements of $\gamma_{\max}$ and $\tau_{\max}$ are available. Again the two inelastic codes differ in their predicted $\gamma_{\max}$ values at shallow depths.

5.2. Sensitivity analysis: Influence of V_s profile

It was shown above that a seemingly small variation at the shear wave velocity profile caused a significantly different response of the soil deposit. One may wonder: how is it possible for such a small variation of V_s profile (165 *vs.* 130 m/s) to result in so different seismic response? And hence, is the proposed

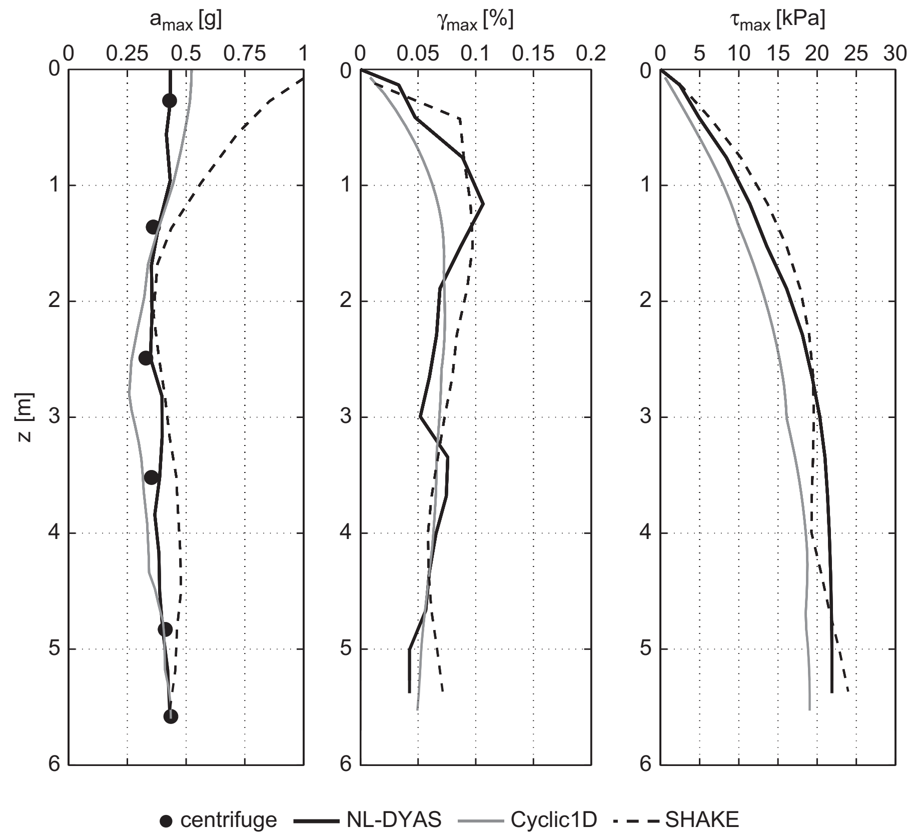

Fig. 17. Distributions of maximum acceleration, shear strain, and shear stress for DKS02 experiment (Revised velocity profile: $V_s=130\ z^{0.25}$; centrifuge acceleration 10 g; shaking with Santa Cruz record, Loma Prieta 1989).

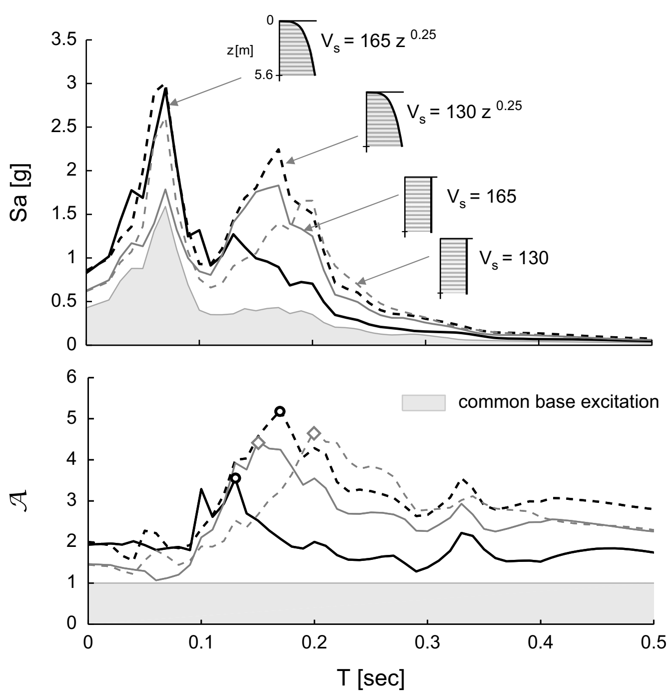

Fig. 18. Investigation of the influence of shear wave velocity profile on the seismic response of a soil profile. Calculated response spectra (top) and spectral ratios (bottom) [shear wave velocities in m/s; excitation: Santa Cruz record, Loma Prieta 1989].

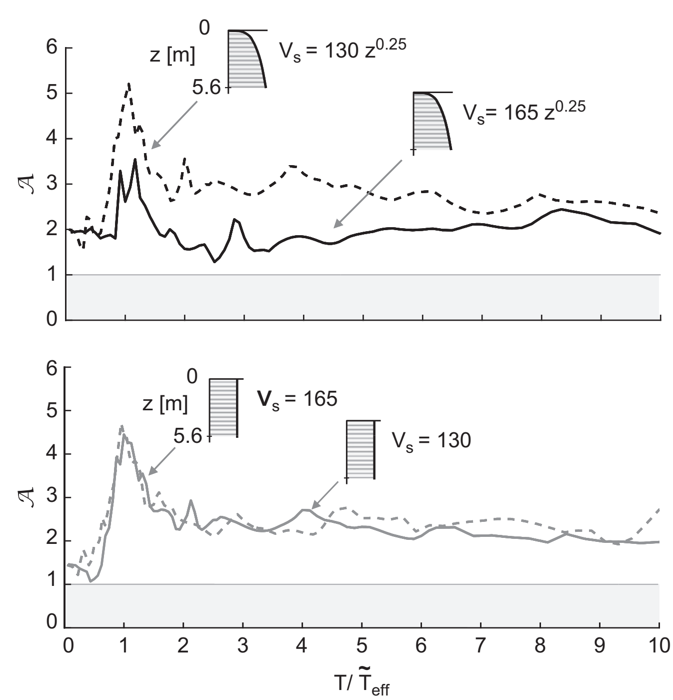

Fig. 19. Investigation of the influence of shear wave velocity profile on the seismic response of a soil profile. Spectral ratios normalized by the effective natural period of the soil deposits [shear wave velocities in m/s ; excitation: Santa Cruz record, Loma Prieta 1989].

revision in V_s the only cause of the discrepancies noticed in Figs. 13–14?

Certainly there can be many combinations of soil profiles and seismic excitations that produce similar amplification of the bedrock motion. Therefore, there are possibly more than one V_s profiles that could give a satisfactory comparison for the case examined above. However, the proposed revision of the V_s profile is believed to be the simplest approximation to reality. Note that the distribution of velocity with the fourth root of depth is well established in the literature for sandy soils, and especially for those created in the controlled conditions of an experiment [2,9,48,1].

Regarding the first question, we attribute the strong sensitivity of the response to the highly inhomogeneous nature of the V_s profile. To support our hypothesis, a simple sensitivity analysis is conducted to investigate the influence of the variation with depth of the soil stiffness on the seismic response of the deposit.

The above examined 5.6-m deep sand deposit is excited by the same motion (Santa Cruz record) and its seismic response is parametrically investigated against different V_s profiles. The previously assumed inhomogeneous profiles (V_s=165 $z^{0.25}$ and V_s=130 $z^{0.25}$) are compared to two homogeneous profiles with the same difference of about 25% (V_s=165 m/s and V_s=130 m/s). Only one set of results (with the equivalent linear model) are compared herein. Similar comparisons were obtained with the other two models. In Fig. 18, the response spectra near the surface (z=0.27 m) computed for the four different profiles are presented along with the corresponding spectral ratios (surface S_a/base S_a). From the two figures it is clear that the difference between the two inhomogeneous profiles is quite significant compared to that of the constant velocity (homogeneous) profiles. The spectral ratios of the latter differ mainly in the period of maximum spectral amplification (0.2 and 0.15 s, approximately) arising from their different natural periods. For the inhomogeneous profiles, the difference is not limited to the (more substantial now) frequency-shifting but there is a noteworthy discrepancy in the amplification too: the stiffer profile (V_s=165 $z^{0.25}$) amplifies the base motion by about 3.5 times while the looser profile (V_s=165 $z^{0.25}$) produces an amplification of more than 5.

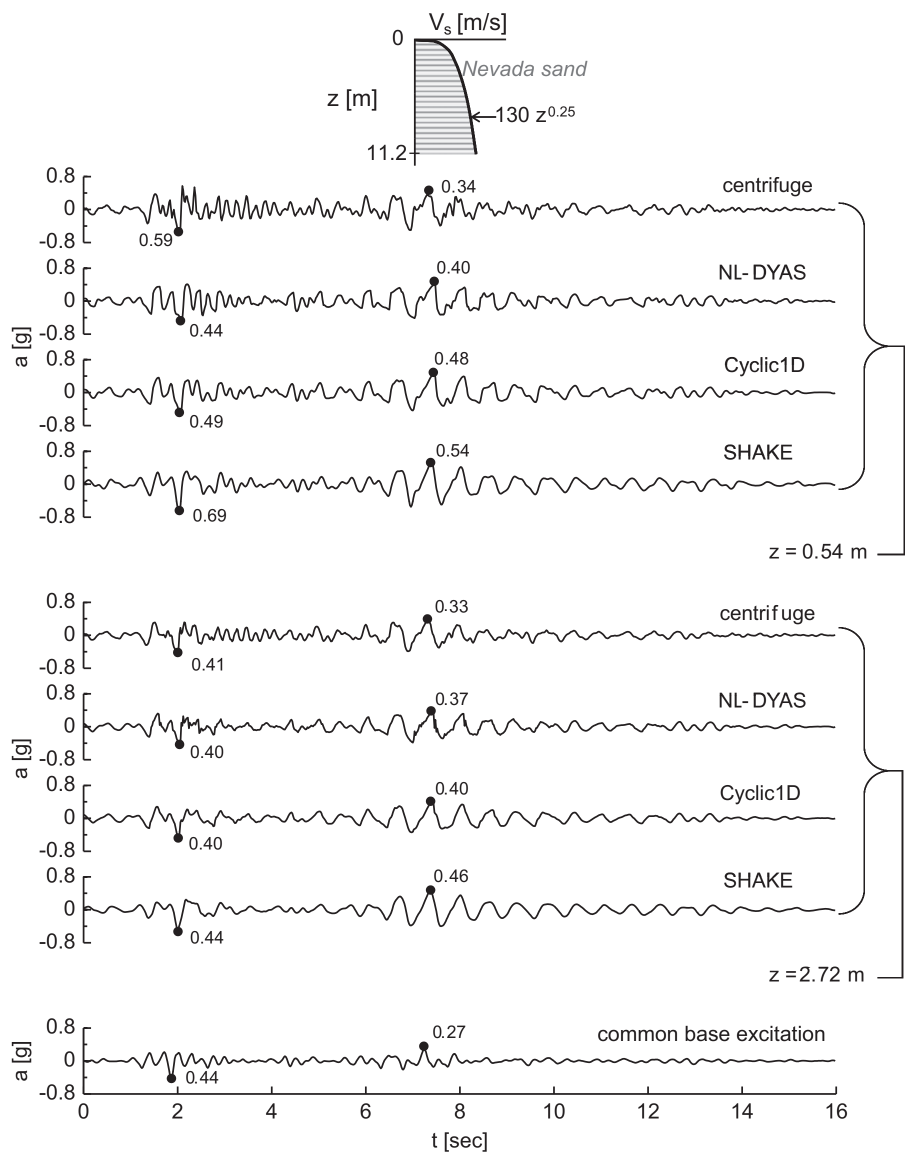

Fig. 20. Comparison of calculated and recorded acceleration time histories for DKS02 experiment (Revised velocity profile: V_s=130 $z^{0.25}$; centrifuge acceleration 20 g; shaking with Santa Cruz record, Loma Prieta 1989).

The differences between the two types of deposits are more vividly illustrated in Fig. 19 where the spectral ratios of the four analyses are plotted *versus* the period ratio $T/\tilde{T}_{eff}$, where $\tilde{T}_{eff}$ is the effective natural period of the deposit, accounting for the level of induced shear strains. Notice the remarkable coincidence of the homogeneous profile amplification functions contrary to the substantial difference of the spectral ratios of the inhomogeneous profiles, almost for all values of the period ratio.

This considerable sensitivity of the response of inhomogeneous profiles to variations in the V_s profile arises, to a certain extend, from the increased significance of the higher eigenmodes of the soil column which is not the case for the homogeneous deposits. This observation is well documented in literature [14,32,1,49].

5.3. Comparisons for the deeper deposit ($H=11.2$ m)

The experiment examined above was repeated in the UC Davis centrifuge facility at a centrifuge acceleration of 20 g, with the same acceleration level at the base: $PGA=0.44$ g.

The results of the three methods are compared with the records in Figs. 20–22. In our analysis, we keep using the revised V_s profile of Eq. (14). The following are some noteworthy observations:

1. All three numerical models produce acceleration histories (near the ground surface and at a depth of 2.72 m) with peaks that are in satisfactory accord with those of the actual motions. In closer look, the two inelastic models give peaks that slightly underpredict the first peaks (0.44–0.49 g *versus* 0.59 g) but overpredict the second peaks (0.40–0.48 g *versus* 0.34 g); the equivalent linear (SHAKE) model results in slightly higher (by up to 20%) peaks.
2. The frequency content of the recorded motions is satisfactorily reproduced with all the three models. SHAKE appears to have spuriously filtered out some of the higher frequencies and especially those of the motion at 2.72 m depth. These observations from the time histories are mirrored in the response spectra of Fig. 21. The inelastic analysis spectra essentially coincide with those "recorded" in the centrifuge, at both locations ($z=0.56$ m and 2.72 m). The equivalent linear spectra overestimate the long-period peak by a factor of nearly 1.4 at the surface and 1.5 at greater depth, while underestimating the short-period peaks, as expected.
3. The distribution of peak ground accelerations with depth reveals a quite acceptable match among centrifuge records and analyses, especially at depths greater than 2 m. Close to the surface, SHAKE slightly overpredicts the ground surface peak value (0.70 g compared to 0.59 g) while the two inelastic codes underestimate the acceleration value by almost the same level (0.49 and 0.44 g *vs.* 0.59 g).
4. Regrettably, an unexpected difference prevailed over our efforts to interpret it: the peak shear strains of the two inelastic models differ appreciably at depth less than 3 m.

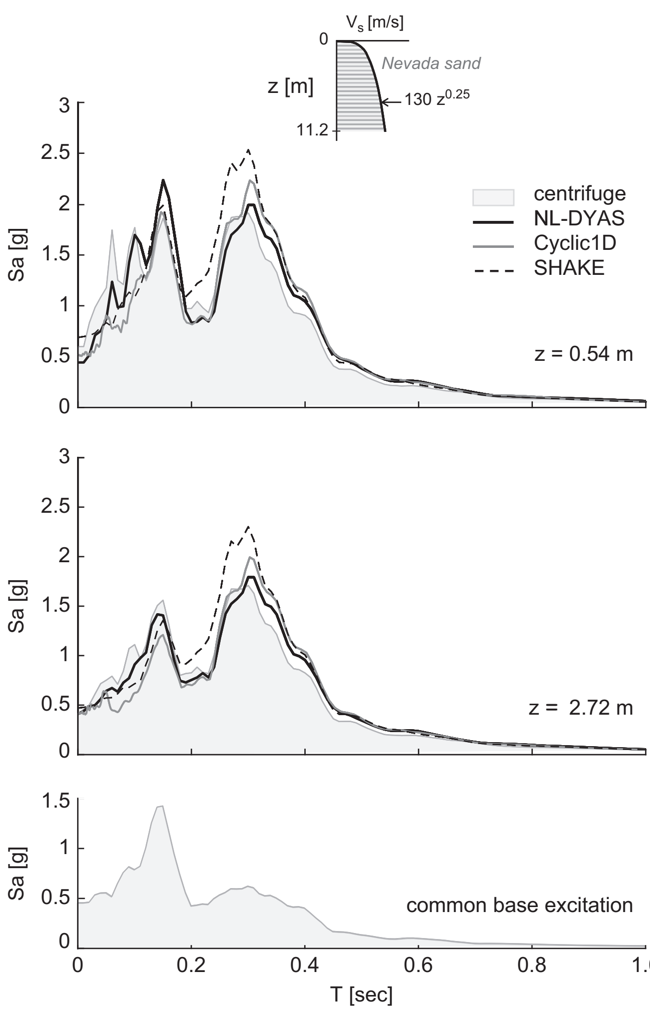

Fig. 21. Comparison of calculated and recorded acceleration response spectra for DKS02 experiment (Revised velocity profile: $V_s=130\ z^{0.25}$; centrifuge acceleration 20 g; shaking with Santa Cruz record, Loma Prieta 1989).

5.4. Comparisons for an extremely severe scenario

In order to investigate the validity of the proposed model and highlight the difference between the nonlinear methods and the equivalent linear one in extreme cases, we repeat the previous analysis applying however a greater acceleration at the bedrock. The 11.2-m deep profile with the revised V_s ($V_s=130\ z^{0.25}$) is excited by the same Santa Cruz record (Loma Prieta 1989 earthquake) scaled up to a peak acceleration of 0.61 g.

The results of the three methods are being compared to each other in Figs. 23–25. The acceleration time histories (Fig. 23) reveal that the inelastic methods (NL-DYAS and Cyclic1D) slightly deamplify the ground motion in the early stages of shaking, apparently as a result of the strong soil nonlinearity developing with the increased base excitation. On the contrary, SHAKE predicts a significant amplification (nearly 1.5 times) of the shaking close to the surface. However, the higher-period peaks at the later stage are amplified by all three methods (more so with SHAKE).

In terms of frequency content there is no substantial difference among the three models. This is reflected in their response spectra (Fig. 24). The two nonlinear models produce practically the same results with a rather minor dissimilarity in the high-frequency range: NL-DYAS predicts somehow greater response than both SHAKE and Cyclic1D at periods lower than 0.12 s. SHAKE results in higher amplification at the fundamental resonance ($T\approx 0.3$ s). In Fig. 25, the profiles of peak acceleration, shear strain, and shear stress are presented. Notice the good accord of the two inelastic codes in the acceleration maxima distribution and the amplification predicted by SHAKE. Again the two inelastic codes differ in their predicted pattern of $\gamma_{\max}$ distribution at shallow depths.

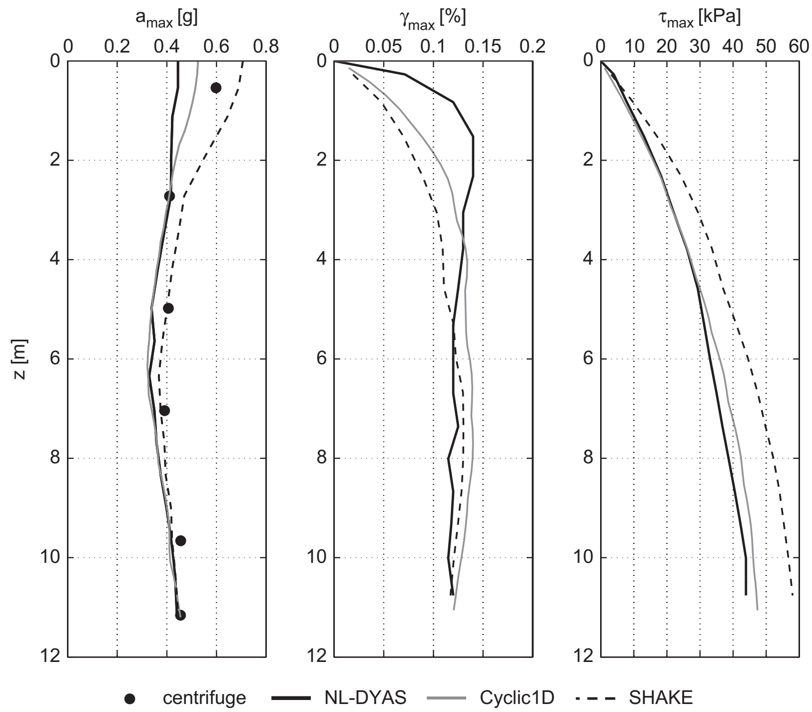

Fig. 22. Distributions of maximum acceleration, shear strain, and shear stress for DKS02 experiment (Revised velocity profile: $V_s = 130\ z^{0.25}$; centrifuge acceleration 20 g; shaking with Santa Cruz record, Loma Prieta 1989).

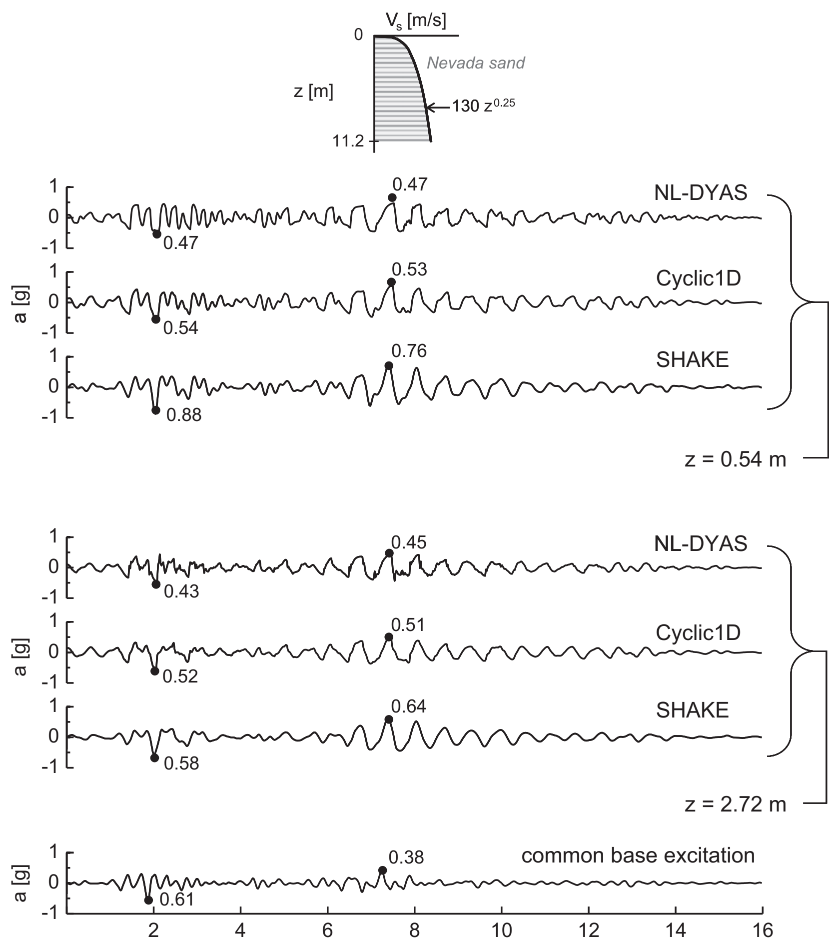

Fig. 23. Comparison of the three calculated acceleration time histories due to a very strong excitation (Velocity profile: $V_s = 130\ z^{0.25}$; excitation: Santa Cruz record at 0.61 g).

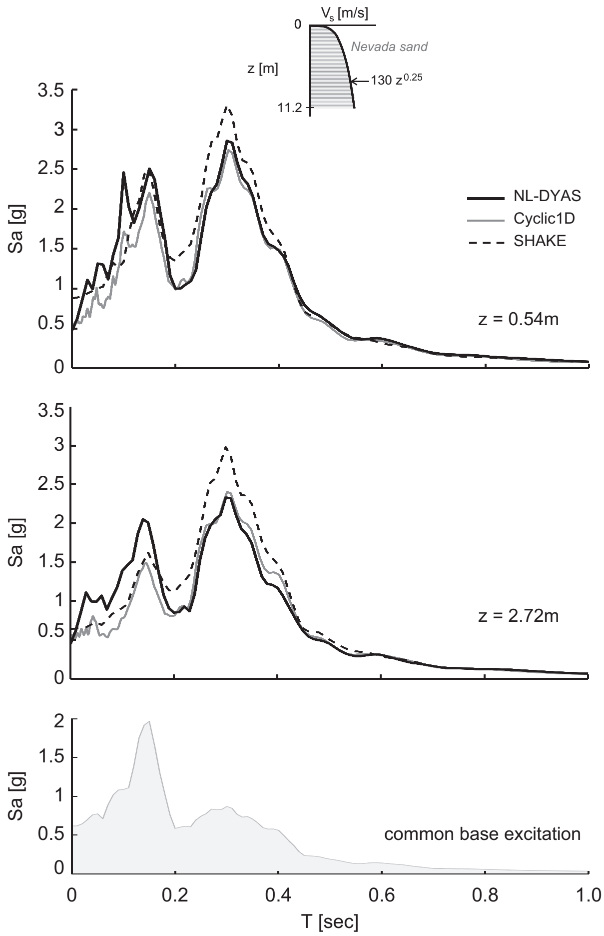

Fig. 24. Comparison of the three calculated acceleration response spectra due to a very strong excitation (Velocity profile: V_s=130 $z^{0.25}$; excitation: Santa Cruz record at 0.61 g).

6. Conclusions

The proposed nonlinear hysteretic model *NL-DYAS* was calibrated in this paper against three widely used sets of G: γ and ξ: γ curves from the literature and a library of model parameter values was assembled so that the user can utilize the new model to analyze 1-D seismic soil response problems. The model was validated against other numerical methods and more significantly against centrifuge experiments. A conclusion of this effort is that the inelastic methods of NL-DYAS (which had been introduced in detail in an earlier publication [[15]) and Cyclic1D (which has been developed by [12] and [13]) proved capable of predicting with sufficient accuracy the soil response to seismic shaking under several different (and *difficult*) circumstances.

As described in the centrifuge test analysis, the accuracy of the prediction is sometimes compromised by the unavoidable uncertainty in soil properties. Hence, proper geotechnical investigation is needed for a realistic ground response analysis. Even the most sophisticated constitutive model would prove inadequate unless soil properties are known reliably.

The equivalent-linear approximation of SHAKE, universally used in practice, produced realistic results, even if somewhat conservative over the results of the truly nonlinear methods and the centrifuge tests. The only (small) exception is at very low periods, where SHAKE underpredicts the motion — an effect of high-frequency overdamping that has been known for quite some time [8,53]. The practical significance of such underprediction is likely to be minor at least for inelastic structures. Overall, in view of the rather extreme soil profiles utilized in this paper (modulus tending to zero at the surface or quite soft clay), the authors conclude that the use of SHAKE in practice is quite justified — especially in view of the ever-present uncertainty on the soil stiffness, and the need for some conservatismin our predictions.

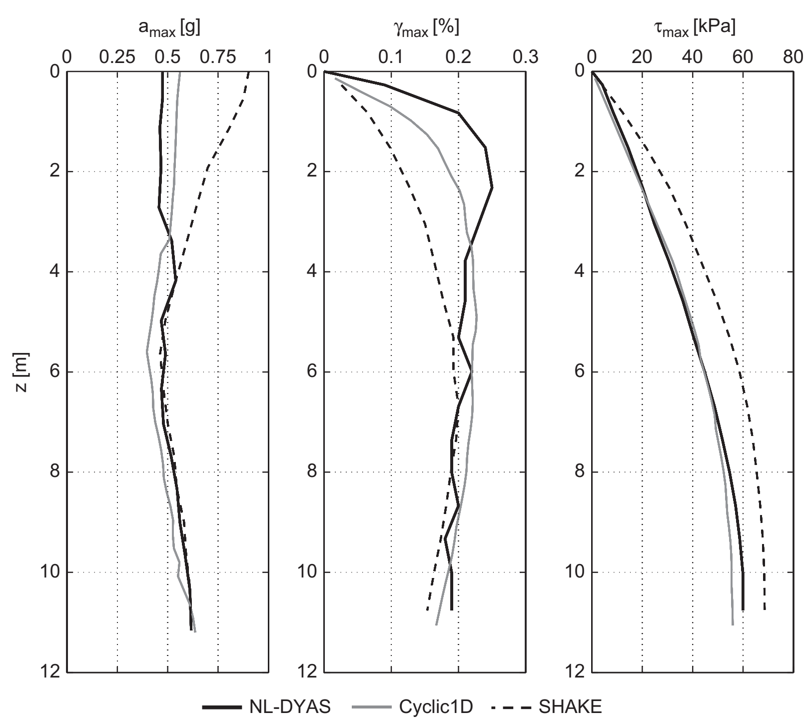

Fig. 25. Distributions of calculated maximum acceleration, shear strain, and shear stress due to a strong excitation (Velocity profile: V_s=130 $z^{0.25}$; excitation: Santa Cruz record at 0.61 g).

Acknowledgment

The financial support for this paper has been provided under the research project "DARE", which is funded through the European Research Council's (ERC) "IDEAS" Program, in Support of Frontier Research–Advanced Grant, under contract/number ERC–2–9–AdG228254–DARE.

References

[1] Afra H, Pecker A. Calculation of free field response spectrum of a non-homogeneous soil deposit from bed rock response spectrum. Soil Dynamics and Earthquake Engineering 2002;22:157–65.
[2] Arulnathan R, Boulanger RW, Kutter BL, Sluis WK. New tool for shear wave velocity measurements in model tests. Geotechnical Testing Journal 2000;23(4):444–53.
[3] Assimaki D, Kausel E. An equivalent linear algorithm with frequency- and pressure-dependent moduli and damping for the seismic analysis of deep sites. Soil Dynamics and Earthquake Engineering 2002;22:959–65.
[4] Assimaki D, Kausel E, Whittle A. Model for dynamic shear modulus and damping for granular soils. Journal of Geotechnical and Geoenvironmental Engineering 2000;126(10):859–69.
[5] Aubry D, Benzenati I, Modaressi, A. Numerical predictions for model No. 1. In: Arulanandan K, Scott RF, editors. Proceedings of the international conference on the verification of numerical procedures for the analysis of soil liquefaction problems. Balkema, Rotterdam, The Netherlands, vol. 1; 1993. pp. 45–66.
[6] Borja RI, Chao HY, Montans F, Lin CH. Nonlinear ground response at Lotung LSST site. Journal of Geotechnical and Geoenvironmental Engineering 1999;125(3):187–97.
[7] Bouc R. Modele mathematique d' hysteresis. Acustica 1971;21:16–25 in [French].
[8] Constantopoulos IV, Roesset JM, Christian JT. A comparison of linear and exact nonlinear analysis of soil amplification,. Proceedings of the 5th World Conference on Earthquake Engineering 1973;2:1806–15.
[9] Dakoulas P, Gazetas G. A class of inhomogeneous shear models for seismic response of dams and embankments,. Soil Dynamics and Earthquake Engineering 1985;4:166–82.
[10] Darendeli MB. Development of a new family of normalized modulus reduction and material damping curves. Doctoral Thesis, Univ of Texas, Austin; 2001.
[11] Darendeli MB, Stokoe KHII, Rathje EM, Roblee, CJ. Importance of confining pressure on nonlinear soil behavior and its impact on earthquake response predictions of deep sites. In: Proceedings of the 15th international conference on soil mechanics and geotechnical engineering. Istanbul, Turkey; August 27–31, 2001.
[12] Elgamal AW, Yang Z, Parra E, Ragheb A. "Cyclic1D: An Internet-based finite element computer program for one-dimensional site amplification analysis using an incremental plasticity coupled solid–fluid (u–p) formulation." Univ. of California, San Diego, (1998) 〈http://cyclic.ucsd.edu〉.
[13] Elgamal AW, Yang Z, Parra E. Computational modeling of cyclic mobility and post-liquefaction site response. Soil Dynamics and Earthquake Engineering 2002;22:259–71.
[14] Gazetas G. Vibrational characteristics of soil deposits with variable wave velocity. International Journal for Numerical and Analytical Techniques in Geomechanics 1982;6:1–20.
[15] Gerolymos N, Gazetas G. Constitutive model for 1-D cyclic soil behavior applied to seismic analysis of layered deposits. Soils and Foundations 2005;45(3):147–59.
[16] Gerolymos N, Gazetas G. Development of Winkler model for static and dynamic response of caisson foundations with soil and interface nonlinearities. Soil Dynamics and Earthquake Engineering 2006;26(5):363–76.
[17] Gerolymos N, Gazetas G. A model for grain-crushing-induced landslides-Application to Nikawa, Kobe 1995. Soil Dynamics and Earthquake Engineering 2007;27(9):803–17.
[18] Hardin BO. The nature of stress–strain behavior of soils. In: Proceedings, earthquake engineering and soil dynamics, ASCE, Pasadena, California, vol. 1, 1978, pp. 3–89.
[19] Hashash YMA. DEEPSOIL. Urbana-Champaign: Tutorial and User Manual. University of Illinois; 2005 vol 2.6.
[20] Hashash Y, Park D. Nonlinear one-dimensional seismic ground motion propagation in the Mississippi embayment. Engineering Geology 2001;62: 185–206.
[21] Ikhouane F, Rodellar J. Systems with Hysteresis: analysis, identification and control using the Bouc–Wen model. New Jersey: John Wiley & Sons Inc.; 2007 pp.202.
[22] Ilankatharan M, Sasaki T, Kutter B, Kramer S, Arduino P. A demonstration of the NEES system for studying soil-foundation-structure interaction. Centrifuge data report for test series MIL01, University of California, Davis; 2005.
[23] Ishibashi I, Zhang X. Unified dynamic shear moduli and damping ratios of sand and clay. Soils and Foundations 1993:182–91.
[24] Ishihara K, Towhata I. One-dimensional soil response analysis during earthquakes based on effective stress model. Journal of Faculty of Engineering, University of Tokyo 1980;35(4).
[25] Jamiolkowski M, Leroueil S, LoPresti DCF. Theme lecture: Design parameters from theory to practice. Proceedings of geo-coast '91, Yokohama, Japan; 1991.
[26] Julier SJ, Uhlmann. A new extension of the Kalman filter to nonlinear systems. In: Proceedings of the 11th international symposium on aerospace/defense sensing, simulation and controls, Orlando, SPIE. Multi Sensor Fusion, Tracking and Resource Management II 1997.
[27] Kausel E, Roesset JM. Soil amplification: some refinements. Soil Dynamics and Earthquake Engineering 1984;3(3):116–23.
[28] Kokusho T. Nonlinear site response and strain-dependent soil properties. Current Science 2004;87(10):1363–9.
[29] Kokusho T, Sato K. Surface-to-base amplification evaluated from KiK-net vertical array strong motion records. Soil Dynamics and Earthquake Engineering 2008;28:707–16.
[30] Lopez-Caballero F, Razavi AM-F, Modaressi H. Nonlinear numerical method for earthquake site response analysis I—elastoplastic cyclic model and parameter identification strategy". Bulletin of Earthquake Engineering 2007;5(3):303–23.
[31] Lo Presti DCF, Lai CG, Puci I. ONDA: computer code for nonlinear seismic response analyses of soil deposits. Journal of Geotechnical and Geoenvironmental Engineering 2006;132(2):223–36.
[32] Lu L, Katayama T, Yamazaki F. Soil amplification based on array observation in Chiba, Japan. In: Prakash S, St Louis, editors. Proceedings of the 2nd international conference on recent advances in geotechnical earthquake engineering and soil dynamics, Missouri, paper no. 8.9. (1991) pp. 1181–8.
[33] Matasovic N. Seismic response of composite horizontally-layered soil deposits, Doctoral Dissertation, University of California, Los Angeles; 1993.
[34] Modaressi A, Lopez-Caballero F. Global methodology for soil behavior identification and its application to the study of site effects. In: Prakash S, editor. Proceedings of the 4th international conference on recent advances in geotechnical earthquake engineering and soil dynamics, San Diego, California, paper no. 1.08 (2001).
[35] Pastor M, Zienkiewicz OC. A generalized plasticity, hierarchical model for sand under monotonic and cyclic loading. In:Pande GN, Van Impe WN, editors. Proceedings of the international symposium on numerical models in geomechanics, M. Jackson & Son, England; 1986.
[36] Pestana JM, Salvati LA. Small-strain behavior of granular soils. I: model for cemented and uncemented sands and gravels,. Journal of Geotechnical and Geoenvironmental Engineering 2006;132(8):1071–81.
[37] Phillips C, Hashash YMA. Damping formulation for nonlinear 1D site response analyses. Soil Dynamics and Earthquake Engineering 2009;29(4): 1143–58.
[38] Prevost JH. A simple plasticity theory for frictional cohesionless soils. Soil Dynamics and Earthquake Engineering 1985;4(1):9–17.
[39] Rathje EM, Kottke AR. Relative differences between equivalent linear nad nonlinear site response methods. In: Proceedings of the 5th international conference on earthquake geotechnical engineering, Santiago, Chile; January 10–13; 2011.
[40] Roesset JM. Soil amplification of earthquakes, Numerical methods in geotechnical engineering, McGraw Hill, Ch. 9, pp. 639–82, 1977.
[41] Sato K, Kokusho T, Matsumoto M, Yamada E. Nonlinear response and soil property during strong motion. Soils and Foundations, Special Issue 1996:41–52.
[42] Schnabel PB, Lysmer J, Seed HB. SHAKE: a computer program for earthquake response analysis of horizontally layered sites. Report EERC 72-12, Earthquake Engineering Research Center, University of California, Berkeley, 1972.
[43] Stevens DK, Kim B-I, Wilson DW, Kutter BL. Comprehensive investigation of nonlinear site response—centrifuge data report for DKS02, Center for Geotechnical Modeling Data Report UCD/CGMDR-99/02, University of California, Davis; 1999.
[44] Stevens DK, Wilson DW, Kutter BL, Kim, BI, Elgamal A Centrifuge model tests to identify dynamic properties of dense sand for site response calculations. In: Prakash S, editor. Proceedings of the 4th international conference on recent advances in geotechnical earthquake engineering and soil dynamics, San Diego; 2001.
[45] Steward JP, Kwok AOL, Hashash YMA, Matasovic N, Pyke R, Wang Z, Yang Z. Benchmarking of nonlinear geotechnical ground response analysis, PEER Report 2008/4, University of California, Berkeley; 2008.
[46] Sugito M, Goda H, Masuda, T, Etsunada K. Equilinearized method with frequency-dependent shear modulus and damping. In: Proceedingsof the 28th Japanese national conference on soil mechanics and foundation engineering, 1993, pp. 1129–32 [in Japanese].
[47] Tokimatsu K, Sekiguchi T. Effects of nonlinear properties of surface soils on strong ground motions recorded in Ojiya during 2004 Mid-Niigata Prefecture earthquake. Soils and Foundations 2006;46(6):765–75.
[48] Towhata I. Seismic wave propagation in elastic soil with continuous variation of shear modulus in the vertical direction. Soils and Foundations 1996;36(1):61–72.
[49] Travasarou T, Gazetas G. On the linear seismic response of soils with modulus varying as a power of depth—the Maliakos marine clay. Soils and Foundations 2004;44(5):85–93.
[50] Vucetic M, Dobry R. Effect of soil plasticity on cyclic response. Journal of Geotechnical Engineering 1991;117(1):89–107.

[51] Wen Y-K. Method for random vibration of hysteretic systems. Journal of Engineering Mechanics 1976;102:249–63.
[52] Yang Z, Elgamal AW, Parra E. Computational model for cyclic mobility and associated shear deformation. Journal of Geotechnical and Geoenvironmental Engineering 2003;129(12):1119–27.
[53] Yoshida N, Kobayashi S, Suetomi I, Miura K. Equivalent linear method considering frequency dependent characteristics of stiffness and damping. Soil Dynamics and Earthquake Engineering 2002;22(3):205–22.
[54] Zambelli C, di Prisco C, d'Onofrio A, Visone C, Santucci de Magistris F. Dependency of the mechanical behavior of granular soils on loading frequency: experimental results and constitutive modeling. In: Ling HI, Callisto L, Leshchinsky D, Koseki J, editors. Soil stress–strain behavior: measurement, modeling and analysis. Geotechnical symposium, Rome, March 16–17, 2006, Springer; 2007, pp. 1016–31.